Complementary opposing D2-MSNs and D1-MSNs dynamics during interval timing

R. Austin Bruce[1], Matthew A. Weber[1], Alexandra S. Bova[1], Rachael A. Volkman[1], Casey E. Jacobs[1], Kartik Sivakumar[1], Hannah R Stutt[1], Young-cho Kim[1], Rodica Curtu[2,3], Nandakumar S. Narayanan[1,3]

[1]Department of Neurology, University of Iowa, [2]Department of Mathematics, University of Iowa, and [3]The Iowa Neuroscience Institute

***Corresponding Author**
Nandakumar Narayanan
nandakumar-narayanan@uiowa.edu
169 Newton Road
Pappajohn Biomedical Discovery Building—5336
University of Iowa, Iowa City, 52242
319-353-5698

Abstract

The role of striatal pathways in cognitive processing is unclear. We studied dorsomedial striatal cognitive processing during interval timing, an elementary cognitive task that requires mice to estimate intervals of several seconds and involves working memory for temporal rules as well as attention to the passage of time. We harnessed optogenetic tagging to record from striatal D2-dopamine receptor-expressing medium spiny neurons (D2-MSNs) in the indirect pathway and from D1-dopamine receptor-expressing MSNs (D1-MSNs) in the direct pathway. We found that D2-MSNs and D1-MSNs exhibited distinct dynamics over temporal intervals as quantified by principal component analyses and trial-by-trial generalized linear models. MSN recordings helped construct and constrain a four-parameter drift-diffusion computational model. This model predicted that disrupting either D2-MSNs or D1-MSNs would increase interval timing response times and alter MSN firing. In line with this prediction, we found that optogenetic inhibition or pharmacological disruption of either D2-MSNs or D1-MSNs increased interval timing response times. Pharmacologically disrupting D2-MSNs or D1-MSNs also changed MSN dynamics and degraded trial-by-trial temporal decoding. Together, our findings demonstrate that D2-MSNs and D1-MSNs make complementary contributions to interval timing despite opposing dynamics, implying that striatal direct and indirect pathways work together to shape temporal control of action. These data provide novel insight into basal ganglia cognitive operations beyond movement and have implications for human striatal diseases and therapies targeting striatal pathways.

62 **Introduction**

63 The basal ganglia have been heavily studied in motor control (Albin et al., 1989). These
64 subcortical nuclei are composed of two pathways defined by medium spiny neurons (MSNs) in
65 the striatum: the indirect pathway, defined by D2-dopamine receptor-expressing MSNs (D2-
66 MSNs), and the direct pathway, defined by D1-dopamine receptor-expressing MSNs (D1-
67 MSNs). It has been proposed that the indirect and direct pathways play opposing roles in
68 movement (Alexander and Crutcher, 1990; Cruz et al., 2022; Kravitz et al., 2010), although
69 recent work identified how these pathways can play more complex and complementary roles
70 (Cui et al., 2013; Tecuapetla et al., 2016). MSNs receive dense input from both motor and
71 cognitive cortical areas (Averbeck et al., 2014; Graybiel, 1997; Middleton and Strick, 2000), but
72 the respective roles of D2-MSNs and D1-MSNs in cognitive processing are largely unknown.
73 Understanding basal ganglia cognitive processing is critical for diseases affecting the striatum
74 such as Huntington's disease, Parkinson's disease, and schizophrenia (Andreasen, 1999; Hinton
75 et al., 2007; Narayanan and Albin, 2022). Furthermore, pharmacological and brain stimulation
76 therapies directly modulate D2-MSNs, D1-MSNs, and downstream basal ganglia structures such
77 as the globus pallidus or subthalamic nucleus. Determining basal ganglia pathway dynamics
78 during cognitive processes will help avoid side effects of current treatments and inspire novel
79 therapeutic directions.

80 We studied striatal D2-MSNs and D1-MSNs during an elementary cognitive task,
81 interval timing, which requires estimating an interval of several seconds. Interval timing provides
82 an ideal platform to study cognition in the striatum because timing 1) requires cognitive
83 resources including working memory for temporal rules and attention to the passage of time

(Parker et al., 2013); 2) is reliably impaired in human striatal diseases such as Huntington's disease, Parkinson's disease, and schizophrenia (Merchant and de Lafuente, 2014); 3) requires nigrostriatal dopamine that modulates MSNs (Emmons et al., 2017; Gouvea et al., 2015; Matell et al., 2003; Mello et al., 2015; Monteiro et al., 2023; Wang et al., 2018); and 4) can be rigorously studied in animal models (Balci et al., 2008; Buhusi and Meck, 2005; Kim et al., 2017a; Parker et al., 2017, 2015). We and others have found that striatal MSNs encode time across multiple intervals by time-dependent ramping activity or monotonic changes in firing rate across a temporal interval (Emmons et al., 2017; Gouvea et al., 2015; Mello et al., 2015; Wang et al., 2018). However, the respective roles of D2-MSNs and D1-MSNs are unknown. Past work has shown that disrupting either D2-dopamine receptors (D2) or D1-dopamine receptors (D1) powerfully impairs interval timing by increasing estimates of elapsed time (Drew et al., 2007; Meck, 2006). Similar behavioral effects were found with systemic (Stutt et al., 2024) or local dorsomedial striatal D2 or D1 disruption (De Corte et al., 2019a). These data lead to the hypothesis that D2 MSNs and D1 MSNs have similar patterns of ramping activity across a temporal interval.

We tested this hypothesis with a combination of optogenetics, neuronal ensemble recording, computational modeling, and behavioral pharmacology. We use a well-described mouse-optimized interval timing task (Balci et al., 2008; Bruce et al., 2021; Larson et al., 2022; Stutt et al., 2024; Tosun et al., 2016; Weber et al., 2023). Strikingly, optogenetic tagging of D2-MSNs and D1-MSNs revealed distinct neuronal dynamics, with D2-MSNs tending to increase firing over an interval and D1-MSNs tending to decrease firing over the same interval, similar to opposing movement dynamics (Cruz et al., 2022; Kravitz et al., 2010; Tecuapetla et al., 2016). MSN dynamics helped construct and constrain a four-parameter drift-diffusion computational

model of interval timing, which predicted that disrupting either D2-MSNs or D1-MSNs would increase interval timing response times. Accordingly, we found that optogenetic inhibition of either D2-MSNs or D1-MSNs increased interval timing response times. Furthermore, pharmacological blockade of either D2- or D1-receptors also increased response times and degraded trial-by-trial temporal decoding from MSN ensembles. Thus, D2-MSNs and D1-MSNs have opposing temporal dynamics yet disrupting either MSN type produced similar effects on behavior. These data demonstrate how striatal pathways play complementary roles in elementary cognitive operations and are highly relevant for understanding the pathophysiology of human diseases and therapies targeting the striatum.

RESULTS

Mouse-optimized interval timing

We investigated cognitive processing in the striatum using a well-described mouse-optimized interval timing task which requires mice to respond by switching between two nosepokes after a 6-second interval (Fig 1A; see Methods; (Balci et al., 2008; Bruce et al., 2021; Larson et al., 2022; Tosun et al., 2016; Weber et al., 2023)). In this task, mice initiate trials by responding at a back nosepoke, which triggers auditory and visual cues for the duration of the trial. On 50% of trials, mice were rewarded for nosepoking after 6 seconds at the designated 'first' front nosepoke; these trials were not analyzed. On the remaining 50% of trials, mice were rewarded for nosepoking at the 'first' nosepoke and then switching to the 'second' nosepoke; initial nosepokes at the second nosepoke after 18 seconds triggered reward when preceded by a first nosepoke. The first nosepokes occurred before switching responses and the second nosepokes occurred much later in the interval in anticipation of reward delivery at 18 seconds (Fig 1B-D). During the task, movement velocity peaked before 6 seconds as mice traveled to the front nosepoke (Fig 1E).

We focused on the *switch response time*, defined as the moment mice exited the first nosepoke before entering the second nosepoke. Switch responses are a time-based decision guided by temporal control of action because mice switch nosepokes only if nosepoking at the first nosepokes does not lead to a reward after 6 seconds (Fig 1B-E). Switch responses are guided by internal estimates of time because no external cue indicates when to switch from the first to the second nosepoke (Balci et al., 2008; Bruce et al., 2021; Tosun et al., 2016; Weber et al., 2023). We defined the first 6 seconds after trial start as the 'interval', because during this epoch mice are estimating whether 6 seconds have elapsed and if they need to switch responses.

In 30 mice, switch response times were 9.3 seconds (8.4 – 9.7; median (IQR)); see Table 1 for a summary of mice, experiments, trials, and sessions). We studied dorsomedial striatal D2-MSNs and D1-MSNs using a combination of optogenetics and neuronal ensemble recordings in 9 transgenic mice (4 D2-Cre mice switch response time 9.7 (7.0 – 10.3) seconds; 5 D1-Cre mice switch response time 8.2 (7.7 – 8.7) seconds; rank sum $p = 0.73$; Table 1).

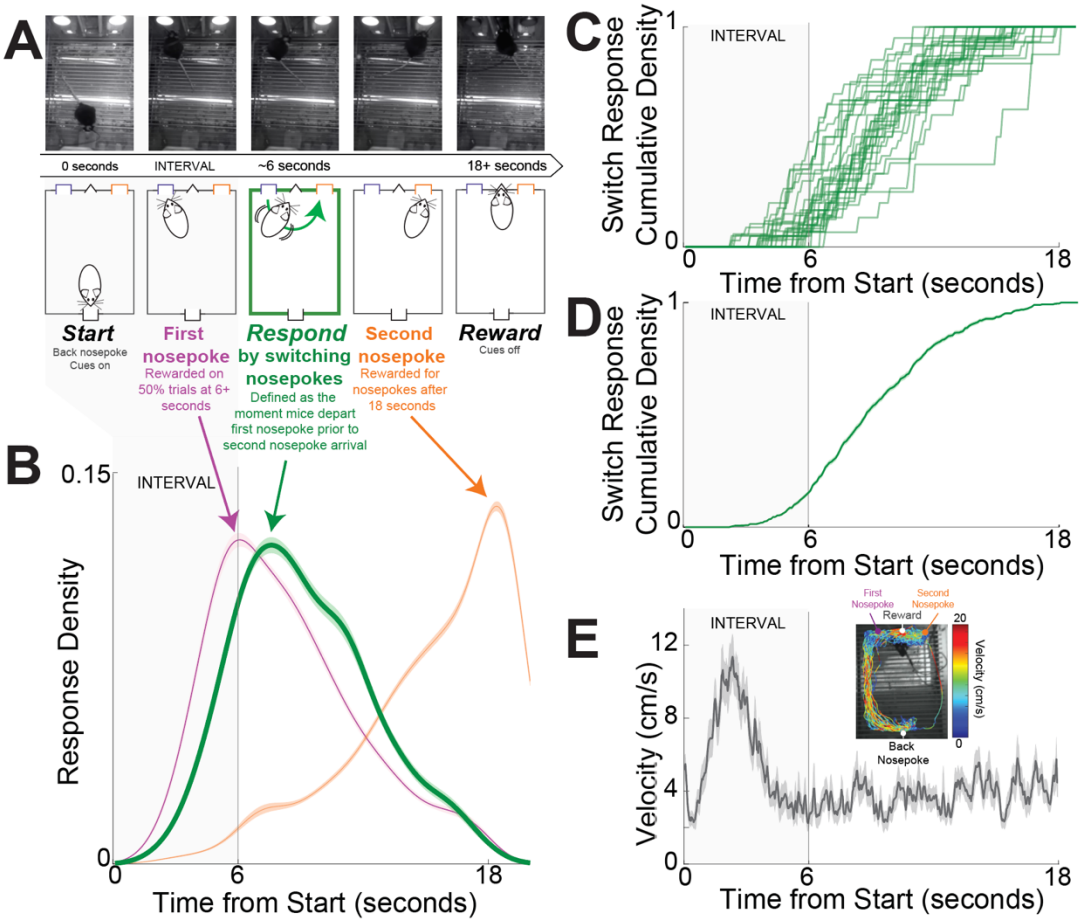

Figure 1: Mouse-optimized interval timing. A) We trained mice to perform an interval timing task in which they had to respond by switching nosepokes after an ~6 second interval (in gray shade in all panels). Mice start trials by making a back nosepoke, which triggers an auditory and visual cue. On 50% of trials, mice were rewarded for a nosepoke after 6 seconds at the designated 'first' front nosepoke; these trials were not analyzed. On the remaining 50% of trials, mice were rewarded for switching to the 'second' nosepoke.; initial nosepokes at the second nosepoke after 18 seconds triggered reward when preceded by a first nosepoke. *Switch response time* was defined as the moment mice depart the first nosepoke prior to second nosepoke arrival. Because cues are identical and on for the full trial on all trials, switch responses are a time-based decision guided explicitly by temporal control of action; indeed, mice switch nosepokes only if they don't receive a reward at the first nosepokes after the 6 second interval. Top row - screen captures from the operant chambers during a trial with switch response. B) Response probability distribution from 30 mice for first nosepokes (purple), switch responses (green), and second nosepokes (orange). Responses at the first nosepoke peaked at 6 seconds, and switch responses peaked after 6 seconds. Because nosepoking at the second nosepoke was only rewarded after 18 seconds, second nosepokes tended to be highly skewed. Shaded area is standard error. C) Cumulative switch response density for each of 30 mice. D) Average cumulative switch response density; shaded area is standard error. E) DeepLabCut tracking of position during interval timing from a single mouse behavioral session revealed increased velocity after trial start and then constant velocity throughout the trial. Shaded area is standard error. In B-E, the 6 second interval is indicated in gray.

146 ***Opposing D2-MSN and D1-MSN dynamics***

147

148 Striatal neuronal populations are largely composed of MSNs expressing D2-dopamine or
149 D1-dopamine receptors. We optogenetically tagged D2-MSNs and D1-MSNs by implanting
150 optrodes in the dorsomedial striatum and conditionally expressing channelrhodopsin (ChR2; Fig
151 S1) in 4 D2-Cre (2 female) and 5 D1-Cre transgenic mice (2 female). This approach expressed
152 ChR2 in D2-MSNs or D1-MSNs, respectively (Fig 2A-B; Kim et al., 2017a). We identified D2-
153 MSNs or D1-MSNs by their response to brief pulses of 473 nm light; neurons that fired within 5
154 milliseconds were considered optically tagged putative D2-MSNs (Fig S1B-C). We tagged 32
155 putative D2-MSNs and 41 putative D1-MSNs in a single recording session during interval
156 timing. There were no consistent differences in overall firing rate between D2-MSNs and D1-
157 MSNs (D2-MSNs: 3.4 (1.4 – 7.2) Hz; D1-MSNs 5.2 (3.1 – 8.6) Hz; F = 2.7, p = 0.11 accounting
158 for variance between mice). Peri-event rasters and histograms from a tagged putative D2-MSN
159 (Fig 2C) and from a tagged putative D1-MSN (Fig 2D) demonstrate prominent modulations for
160 the first 6 seconds of the interval after trial start. Z-scores of average peri-event time histograms
161 (PETHs) from 0 to 6 seconds after trial start for each putative D2-MSN are shown in Fig 2E and
162 for each putative D1-MSN in Fig 2F. These PETHs revealed that for the 6-second interval
163 immediately after trial start, many putative D2-MSN neurons appeared to ramp up while many
164 putative D1-MSNs appeared to ramp down. For 32 putative D2-MSNs average PETH activity
165 increased over the 6-second interval immediately after trial start, whereas for 41 putative D1-
166 MSNs, average PETH activity decreased. These differences resulted in distinct activity early in
167 the interval (0-1 seconds; F = 6.0, p = 0.02 accounting for variance between mice), but not late in
168 the interval (5-6 seconds; F = 1.9, p = 0.17 accounting for variance between mice) between D2-
169 MSNs and D1-MSNs. Examination of a longer interval of 10 seconds before to 18 seconds after

trial start revealed the greatest separation in D2-MSN and D1-MSN dynamics during the 6-second interval after trial start (Fig S2). Strikingly, these data suggest that D2-MSNs and D1-MSNs might display opposite dynamics during interval timing.

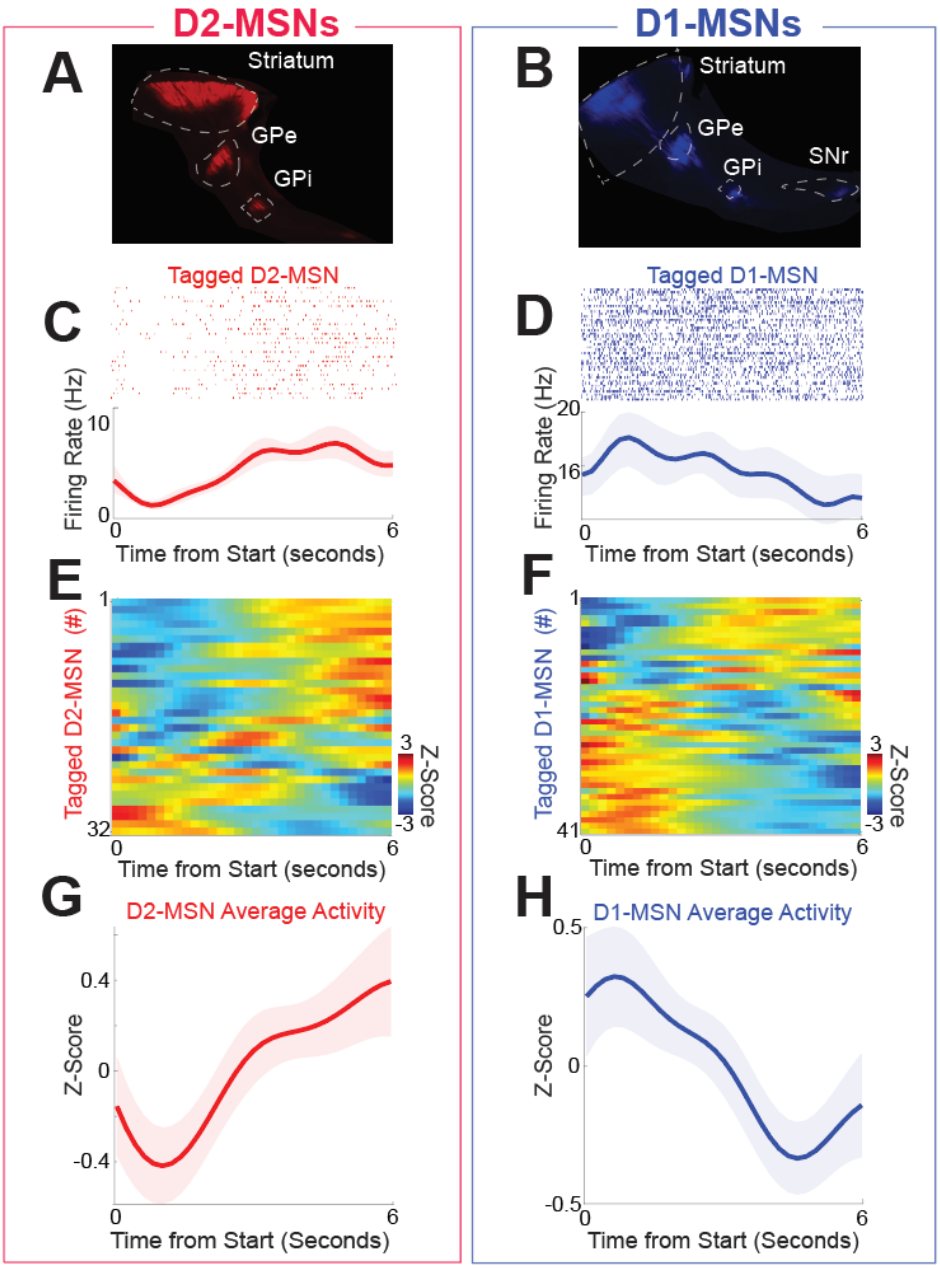

Figure 2: D2-MSNs and D1-MSNs have opposing dynamics during interval timing. A) D2-MSNs in the indirect pathway, which project from the striatum to the globus pallidus external segment (GPe; sagittal section) and internal segment (GPi) and B) D1-MSNs, which project from the striatum to the GPe, GPi, and substantia nigra (SNr; sagittal section). Peri-event raster C) from an optogenetically tagged putative D2-MSN (red) and D) from an optogenetically tagged putative D1-MSN (blue). Shaded area is the bootstrapped 95% confidence interval. E) Peri-event time histograms (PETHS) from all D2-MSNs and F) from all D1-MSNs. were binned at 0.2 seconds, smoothed using kernel-density estimates using a bandwidth of 1, and z-scored. Average activity from PETHs revealed that G) D2-MSNs (red) tended to ramp up, whereas H) D1-MSNs (blue) tended to ramp down. Shaded area is standard error. Data from 32 tagged D2-MSNs in 4 D2-Cre mice and 41 tagged D1-MSNs in 5 D1-Cre mice.

176 ***Differences between D2-MSNs and D1-MSNs***

177 To quantify differences between D2-MSNs vs D1-MSNs, we turned to principal
178 component analysis (PCA), a data-driven tool to capture the diversity of neuronal activity (Kim
179 et al., 2017a). Work by our group and others has uniformly identified PC1 as a linear component
180 among corticostriatal neuronal ensembles during interval timing (Bruce et al., 2021; Emmons et
181 al., 2020, 2019, 2017; Kim et al., 2017a; Narayanan et al., 2013; Narayanan and Laubach, 2009;
182 Parker et al., 2014; Wang et al., 2018). We analyzed PCA calculated from all D2-MSN and D1-
183 MSN PETHs over the 6-second interval immediately after trial start. PCA identified time-
184 dependent ramping activity as PC1 (Fig 3A), a key temporal signal that explained 54% of
185 variance among tagged MSNs (Fig 3B; variance for PC1 p = 0.009 vs 46 (44-49)% variance for
186 PC1 derived from random data; Narayanan, 2016). In line with population averages from Fig
187 2G&H, D2-MSNs and D1-MSNs had opposite patterns of activity with negative PC1 scores for
188 D2-MSNs and positive PC1 scores for D1-MSNs (Fig 3C; PC1 for D2-MSNs: -3.4 (-4.6 – 2.5);
189 PC1 for D1-MSNs: 2.8 (-2.8 – 4.9); F = 8.8, p = 0.004 accounting for variance between mice
190 (Fig S3A); Cohen's d = 0.7; power = 0.80; no reliable effect of sex (F = 0.44, p = 0.51) or
191 switching direction (F = 1.73, p = 0.19)). Thus, analysis of PC1, which exhibited time-dependent
192 ramping similar to D2-MSN/D1-MSN average activity (Fig 2G/H and Fig S2C), S2E suggested
193 that D2-MSNs and D1-MSNs had opposing ramping dynamics.

194 To interrogate these dynamics at a trial-by-trial level, we calculated the linear slope of
195 D2-MSN and D1-MSN activity over the first 6 seconds of each trial using generalized linear
196 modeling (GLM) of effects of time in the interval vs trial-by-trial firing rate (Latimer et al.,
197 2015). Nosepokes were included as a regressor for movement. GLM analysis also demonstrated
198 that D2-MSNs had significantly different slopes (-0.01 spikes/second (-0.10 – 0.10)), which were

199 distinct from D1-MSNs (-0.20 (-0.47– -0.06; Fig 3D; F = 8.9, p = 0.004 accounting for variance
200 between mice (Fig S3B); Cohen's d = 0.8; power = 0.98; no reliable effect of sex (F = 0.02, p =
201 0.88) or switching direction (F = 1.72, p = 0.19)). We found that D2-MSNs and D1-MSNs had
202 significantly different slopes even when excluding outliers (4 outliers excluded outside of 95%
203 confidence intervals; F = 7.51, p = 0.008 accounting for variance between mice) and when the
204 interval was defined as the time between trial start and the switch response on a trial-by-trial
205 basis for each neuron (F = 4.3, p = 0.04 accounting for variance between mice). Trial-by-trial
206 GLM slope was correlated with PC1 scores in Fig 3A-C (PC1 scores vs. GLM slope r = -0.60, p
207 = 10^{-8}). These data demonstrate that D2-MSNs and D1-MSNs had distinct slopes of firing rate
208 across the interval and were consistent with analyses of average activity and PC1, which
209 exhibited time-related ramping.

210 Our findings could not be easily explained by movement because 1) few responses
211 occurred before 6 seconds (23%) and 44% of tagged neurons were recorded in trials without a
212 single nosepoke before 6 seconds (Fig 1B-C), 2) our GLM included a regressor accounting for
213 the nosepokes when present, and 3) nosepoke GLM βs were not reliably different between D2-
214 MSNs and D1-MSNs (F = 1.5, p = 0.22 accounting for variance between mice).

215 In summary, we used optogenetic tagging to record from D2-MSNs and D1-MSNs
216 during interval timing. Analyses of average activity, PC1, and trial-by-trial firing-rate slopes
217 over the interval provide convergent evidence that D2-MSNs and D1-MSNs had distinct and
218 opposing dynamics during interval timing. These data provide insight into temporal processing
219 by striatal MSNs.

220

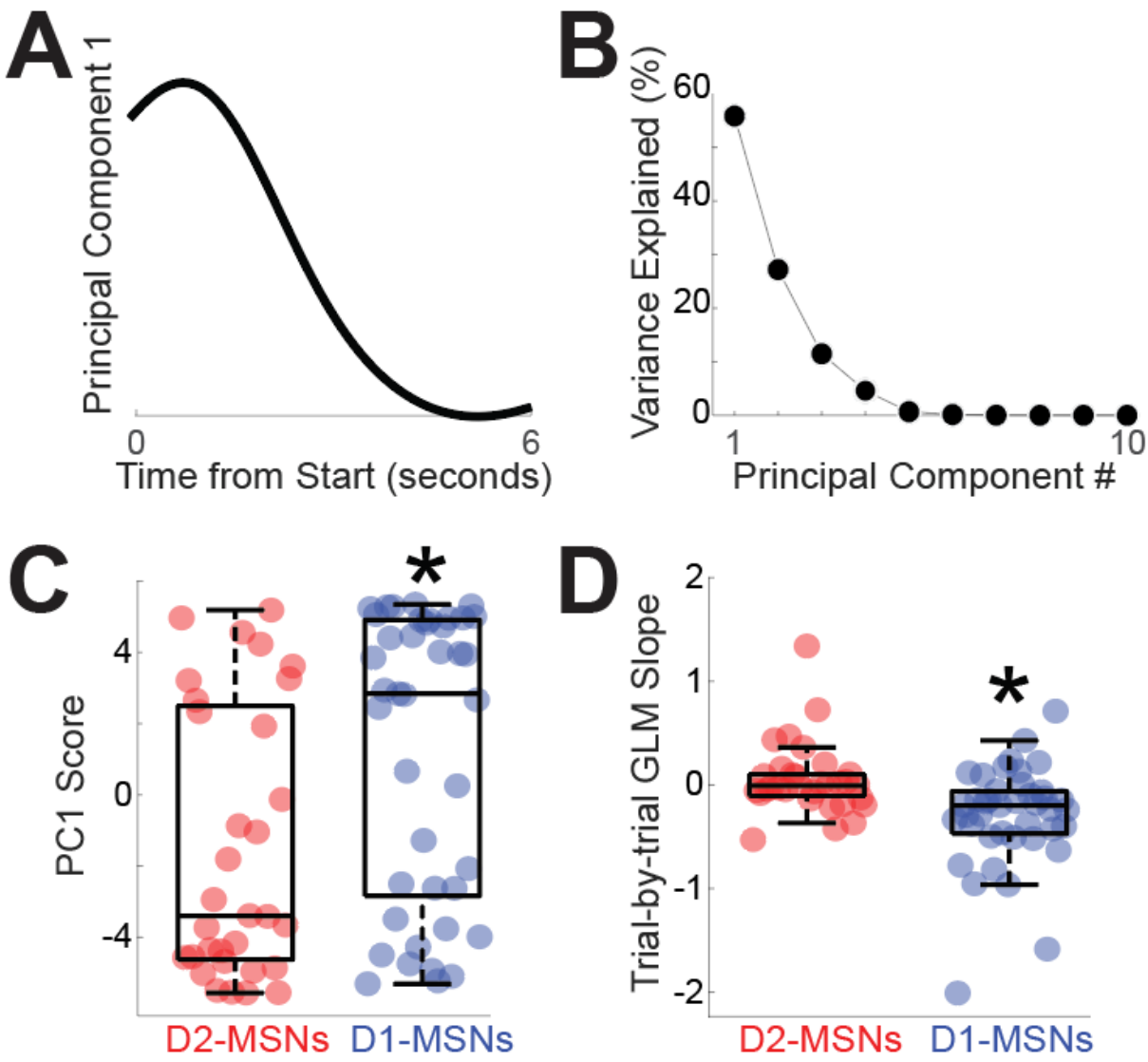

Figure 3: Quantification of opposing D2-MSN and D1-MSN dynamics A) Principal component analysis revealed that the first component (PC1) exhibited time-dependent ramping. B) The first principal component explained ~54% of variance across tagged MSN ensembles. C) Differences between D2-MSNs (red) and D1-MSNs (blue) were captured by PC1 which exhibited time-dependent ramping. D) These differences were also apparent in the linear slope of firing rate vs time in the interval, with D1-MSNs (blue) having a more negative slope than D2-MSNs (red). In C and D, each point represents data from a tagged MSN. * = $p < 0.05$ via linear mixed effects models accounting for variance between mice. Data from 32 tagged D2-MSNs in 4 D2-Cre mice and 41 tagged D1-MSNs in 5 D1-Cre mice.

Drift-diffusion models of opposing D2-MSN and D1-MSN dynamics

Our data demonstrate that D2-MSNs and D1-MSNs have opposite activity patterns. However, past computational models of interval timing have relied on drift-diffusion dynamics with a positive slope that accumulates evidence over time (Nguyen et al., 2020; Simen et al., 2011). To reconcile how these MSNs might complement to effect temporal control of action, we constructed a four-parameter drift-diffusion model (DDM). Our goal was to construct a DDM inspired by average differences in D2-MSNs and D1-MSNs that predicted switch-response time behavior. We constructed a DDM where x represents the neuronal firing rate of an 'output' unit collecting evidence on the activity of striatal D2-MSNs or D1-MSNs, t represents time measured in seconds, and dx and dt mean "change" in x and t respectively (equivalent to the derivative dx/dt):

$$dx = (F - x)Ddt + \sigma d\xi(t) \qquad \text{(Equation 1)}$$

$$x(0) = b \qquad \text{(Equation 2)}$$

The model has four independent parameters F, D, σ, and b (described below) and a threshold value T defined by

$$T = T(F, b) = \left(1 - \frac{1}{4}b\right)F + \frac{1}{4}b(1 - F) \qquad \text{(Equation 3)}$$

The firing rate is set initially at baseline b (see Equation 2), then driven by input F akin to the dendritic current induced by the overlap of corticostriatal postsynaptic potentials (Shepherd, 2013). With each unit of time *dt*, we suppose there is corticostriatal stimulation that provides incremental input proportional to the activity itself, $(F - x)D$, to reach a decision. D is *the drift rate* for the event sequence and can be interpreted as a parameter inverse proportional to the neural activity's integration time constant. The drift, together with noise $\xi(t)$ (of zero mean and

strength σ), leads to fluctuating accumulation which eventually crosses a threshold T (see Equation 3; Fig 4A-B). The time t^* it takes the firing rate to reach the threshold, $x(t^*) = T$, is the *switch response time*.

Our model aimed to fit statistical properties of mouse behavioral responses while incorporating MSN network dynamics. However, the model does not attempt to fit individual neurons' activity, because our model predicts a single behavioral parameter – switch time – that can be caused by the aggregation of diverse neuronal activity. We first analyzed trial-based aggregated activity of MSN recordings from each mouse ($x_j(t)$) where $j = 1, \dots, N$ neurons. For D2-MSN or D1-MSN ensembles of $N > 11$, we found linear combinations of their neuronal activities, with some β_j coefficients,

$$x(t) = \sum_{j=1}^{N} \beta_j \, x_j(t)$$

that could predict the trial-by-trial switch response times (accuracy > 90%, Fig S4; compared with < 20% accuracy for Poisson-generated spikes of same trial-average firing rate). The predicted switch time t^*_{pred} was defined by the time when the weighted ensemble activity $x(t)$ first reached the value $x(t^*_{pred})$ = 0.5. Finally, we built DDMs to account for this opposing trend (increasing vs decreasing) of MSN dynamics and for ensemble threshold behavior defining t^*_{pred}; see the resulting model (Equations 1-3) and its simulations (Figure 4A-B).

This instantiation of DDMs captured the complimentary D2-MSN and D1-MSN dynamics that we discovered in our optogenetic tagging experiments (Fig 2G-H vs. 4A-B). The model's parameters were chosen to fit the distribution of switch response times: $F = 1, b = 0.52$

(so $T = 0.87$), $D = 0.135, \sigma = 0.052$ for intact D2-MSNs (Fig 4A, in black); and $F = 0, b = 0.48$ (so $T = 0.13$), $D = 0.141, \sigma = 0.052$ for intact D1-MSNs (Fig 4B, in black). Interestingly, we observed that two-parameter gamma distributions almost perfectly accounted for the model dynamics (D2-MSNs: Gamma parameters $\alpha = 6.08$, $\beta = 0.69$, R^2 vs Model = 0.99; D1-MSNs $\alpha = 5.89$, $\beta = 0.69$; R^2 vs Model = 0.99; Fig 4C-D, dotted black lines). Gamma distributions provided a surprisingly good approximation for the probability distribution and cumulative distribution functions of mouse switch response times (Fig 1B-D). Thus, in the next sections, we used gamma distributions as a proxy for both the distribution of times generated by the model and the distribution of mice switch response times when comparing those for the goodness of fit. Our model provided the opportunity to computationally explore the consequences of disrupting D2-MSNs or D1-MSNs. Because both D2-MSNs and D1-MSNs accumulate temporal evidence, disrupting either MSN type in the model changed the slope. The results were obtained by simultaneously decreasing the drift rate D (equivalent to lengthening the neurons' integration time constant) and lowering the level of network noise σ: $D = 0.129, \sigma = 0.043$ for D2-MSNs in Fig 4A (in red; changes in noise had to accompany changes in drift rate to preserve switch response time variance); and $D = 0.122, \sigma = 0.043$ for D1-MSNs in Fig 4B (in blue). The model predicted that disrupting either D2-MSNs or D1-MSNs would increase switch response times (Fig 4C and Fig 4D) and would shift MSN dynamics. In the next section, we interrogated these ideas with a combination of optogenetics, behavioral pharmacology, and electrophysiology.

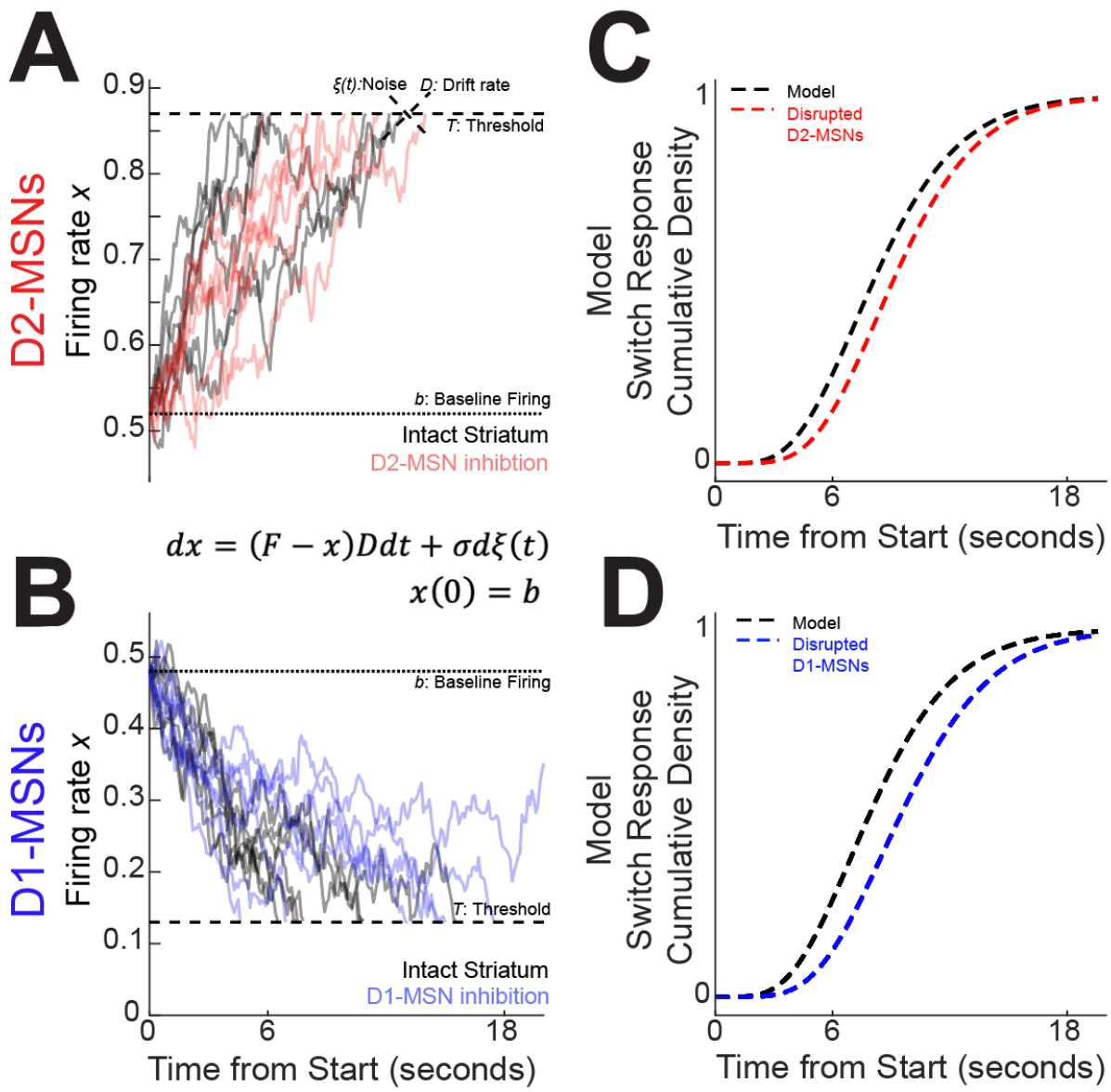

Figure 4: Four-parameter drift-diffusion computational model of striatal activity during interval timing. A) We modeled interval timing with a low parameter diffusion process with a drift rate *D*, noise $\xi(t)$, and a baseline firing rate *b* that drifts toward a threshold *T* indicated by dotted lines. With D2-MSNs disrupted (solid red curves), this drift process decreases in slope and takes longer to reach the threshold. B) The same model also accounted for D1-MSNs with an opposite drift slope. With D1-MSNs disrupted (solid blue curves), the drift process again takes longer to reach the threshold. Because both D2-MSNs and D1-MSNs contribute to the accumulation of temporal evidence, this model predicted that C) disrupting D2-MSNs would increase response times during interval timing (dotted red line) and D) disrupting D1-MSNs would also increase response times (dotted blue line). Threshold *T* depends on *b* and target firing *F*.

290 ***Disrupting D2-MSNs or D1-MSNs increases switch response times***

291 DDMs captured opposing MSN dynamics and predicted that disrupting either D2-MSNs
292 or D1-MSNs should slow temporal processing and increase switch response times (Fig 4). We
293 tested this idea with optogenetics. We bilaterally implanted fiber optics and virally expressed the
294 inhibitory opsin halorhodopsin in the dorsomedial striatum of 10 D2-Cre mice (5 female) to
295 inhibit D2-MSNs (Fig S5; this group of mice was entirely separate from the optogenetic tagging
296 mice). We found that D2-MSN inhibition reliably increased switch response times (Fig 5A-B;
297 Laser Off: 8.6 seconds (8.3–9.3); Laser On: 10.2 seconds (9.4–10.2); signed rank $p = 0.002$,
298 Cohen's $d = 1.7$). Importantly, we found no reliable effects for D2-MSNs with opsin-negative
299 controls (Fig S6). Remarkably, DDM predictions were highly concordant with D2-MSN
300 inhibition behavioral data ($R^2 = 0.55$; parameters chosen to fit D2-MSN inhibition trials) as well
301 as with behavioral data from laser-off trials ($R^2 = 0.63$; parameters chosen to fit laser-off trials;
302 Fig S7).

303 Next, we investigated D1-MSNs (Kravitz et al., 2010). In 6 D1-Cre mice (3 female),
304 optogenetic inhibition of dorsomedial striatal D1-MSNs increased switch response times (Fig
305 5C-D; Laser Off: 8.7 (8.0–9.1) seconds; Laser On: 10.5 (9.6 – 11.1) seconds; signed rank $p =$
306 0.03, Cohen's $d = 1.4$). As with D2-MSNs, we found no reliable effects with opsin-negative
307 controls in D1-MSNs (Fig S6). DDM predictions again were highly concordant with D1-MSN
308 inhibition behavioral data ($R^2 = 0.56$; parameters chosen to fit D1-MSN inhibition trials) and
309 with laser off trials ($R^2 = 0.64$; parameters chosen to fit laser off trials; Fig S7).

310 To test the generality of the effects observed in the optogenetic inhibition experiment, we
311 turned to systemic pharmacology. We used sulpiride (12.5 mg/kg intraperitoneally (IP)) to block
312 D2-dopamine receptors in 10 wild-type (WT) mice, which increased switch response times

relative to saline sessions (median (IQR); saline: 8.9 (8.4 – 9.8) seconds; D2 blockade: 10.1 (9.4 – 10.8) seconds; signed rank $p = 0.002$, Cohen's $d = 1.0$; Fig 5E-F). Of note, there was no difference in switch response time between saline sessions and laser-off trials from D2-MSN optogenetic inhibition in D2-Cre mice, implying that in optogenetic sessions, D2-MSN inhibition did not disrupt behavior during laser-off trials (rank sum $p = 0.31$). These data are consistent with past work demonstrating that disrupting dorsomedial D2-MSNs slows timing (De Corte et al., 2019b; Drew et al., 2007; Stutt et al., 2024). In the same 10 wild-type mice, systemic drugs blocking D1-dopamine receptors (D1 blockade; SCH23390 0.05 mg/kg IP) increased switch response times (saline: 9.7 seconds (9.0 – 9.9); D1 blockade: 10.1 seconds (9.3 – 11.4); signed rank $p = 0.04$, Cohen $d = 0.7$; Fig 5G-H). Once again, there was no difference between saline sessions and D1-MSN inhibition laser-off trials in D1-Cre mice (rank sum $p = 0.18$). These results are in line with our DDM predictions and demonstrate that disrupting either D2-MSNs or D1-MSNs increases switch response time.

We found no evidence that inhibiting D2-MSNs in the dorsomedial striatum changed task-specific movements such as nosepoke duration (i.e., time of nosepoke entry to exit; signed rank $p = 0.63$; Fig S8 for the 10 D2-Cre mice in optogenetics trials) or switch traversal time between the first and second nosepokes (signed rank $p = 0.49$; Fig S8). Similarly, we found no evidence that D1-MSN inhibition changed nosepoke duration (signed rank $p = 0.31$; Fig S8 for the 6 D1-Cre mice) or traversal time (signed rank $p = 0.22$; Fig S8). Furthermore, disrupting D2-MSNs or D1-MSNs did not change switch response time standard deviations or the number of rewards (Fig S9). These results demonstrate that disrupting dorsomedial striatal D2-MSNs and D1-MSNs specifically slowed interval timing without consistently changing task-specific movements.

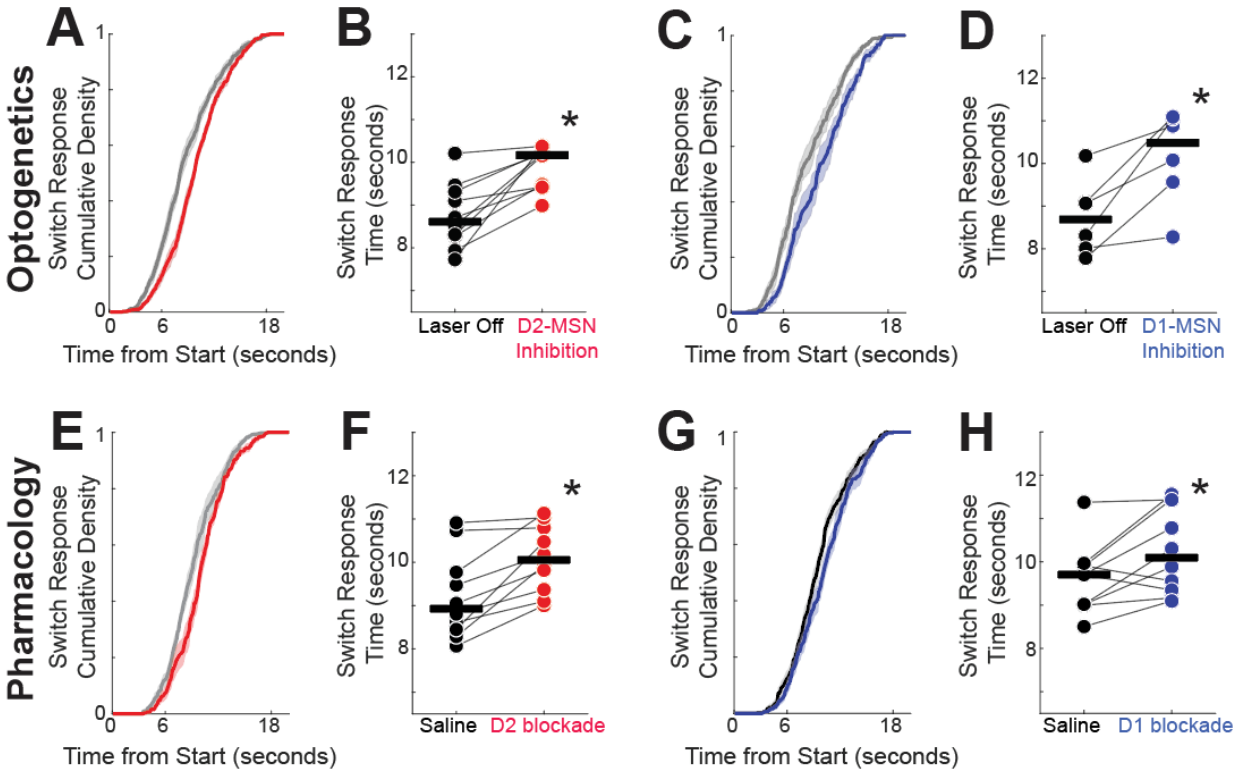

Figure 5: Disrupting D2- or D1-MSNs increases response times. A) As predicted by our DDM in Fig 4, optogenetic inhibition of D2-MSNs (red) shifted cumulative distributions of response times to the right, and B) increased response times; data from 10 D2-Cre mice expressing halorhodopsin (Halo). Also as predicted by our DDM, C) optogenetic inhibition of D1-MSNs shifted cumulative distribution functions to the right, and D) increased response times; data from 6 D1-Cre mice expressing Halo. Similarly, E) pharmacologically disrupting D2-dopamine receptors (red) with the D2 antagonist sulpiride shifted cumulative distribution functions to the right, and F) increased response times; data from 10 wild-type mice. Also, G) pharmacologically disrupting D1-dopamine receptors (blue) with the D1 antagonist SCH23390 shifted cumulative distribution functions to the right, and H) increased response times; data from the same 10 wild-type mice as in E-F. In B, D, F, and H connected points represent the mean response time from each animal in each session, and horizontal black lines represent group medians. *$p = < 0.05$, signed rank test. See Figure S6 for data from opsin-negative controls.

342 ***D2 blockade and D1 blockade shift MSN dynamics***

343 MSN ensembles strongly encode time (Bruce et al., 2021; Emmons et al., 2017; Gouvea
344 et al., 2015; Mello et al., 2015; Wang et al., 2018), but it is unknown how disruptions in D2-
345 dopamine or D1-dopamine receptors affect these ensembles (Yun et al., 2023). Although non-
346 specific, pharmacological experiments have two advantages over optogenetics for recording
347 experiments: 1) many clinically approved drugs target dopamine receptors, and 2) they are more
348 readily combined with recordings than optogenetic inhibition, which silences large populations
349 of MSNs. We recorded from dorsomedial striatal MSN ensembles in 11 separate mice during
350 sessions with saline, D2 blockade with sulpiride, or D1 blockade with SCH23390 (Fig 6A; Fig
351 S10; data from one recording session each for saline, D2 blockade, and D1 blockade during
352 interval timing).

353 We analyzed 99 MSNs in sessions with saline, D2 blockade, and D1 blockade. We
354 matched MSNs across sessions based on waveform and interspike intervals; waveforms were
355 highly similar across sessions (correlation coefficient between matched MSN waveforms: saline
356 vs D2 blockade r = 1.00 (0.99 – 1.00 rank sum vs correlations in unmatched waveforms p =
357 $3x10^{-44;}$ waveforms; saline vs D1 blockade r = 1.00 (1.00 – 1.00), rank sum vs correlations in
358 unmatched waveforms $p = 4x10^{-50}$). There were no consistent changes in MSN average firing
359 rate with D2 blockade or D1 blockade (F = 1.1, p = 0.30 accounting for variance between
360 MSNs; saline: 5.2 (3.3 – 8.6) Hz; D2 blockade 5.1 (2.7 – 8.0) Hz; F = 2.2, p = 0.14; D1 blockade
361 4.9 (2.4 – 7.8) Hz).

362 We noticed differences in MSN activity across the interval with D2 blockade and D1
363 blockade at the individual MSN level (Fig 6B-D) as well as at the population level (Fig 6E). We
364 used PCA to quantify effects of D2 blockade or D1 blockade (Bruce et al., 2021; Emmons et al.,
365 2017; Kim et al., 2017a). We constructed principal components (PC) from z-scored peri-event

366 time histograms of firing rate from saline, D2 blockade, and D1 blockade sessions for all mice
367 together. The first component (PC1), which explained 54% of neuronal variance, exhibited
368 "time-dependent ramping", or monotonic changes over the 6 second interval immediately after
369 trial start (Fig 6F-G; variance for PC1 $p = 0.001$ vs 46 (45-47)% variance in random data;
370 Narayanan, 2016). Interestingly, PC1 scores shifted with D2 blockade (Fig 6F; PC1 scores for
371 D2 blockade: -0.6 (-3.8 – 4.7) vs saline: -2.3 (-4.2 – 3.2), $F = 5.1$, $p = 0.03$ accounting for
372 variance between MSNs; no reliable effect of sex ($F = 0.2$, $p = 0.63$) or switching direction ($F =$
373 2.8, $p = 0.10$)). PC1 scores also shifted with D1 blockade (Fig 6F; PC1 scores for D1 blockade: -
374 0.0 (-3.9 – 4.5), $F = 5.8$, $p = 0.02$ accounting for variance between MSNs; no reliable effect of
375 sex ($F = 0.0$, $p = 0.93$) or switching direction ($F = 0.9$, $p = 0.34$)). There were no reliable
376 differences in PC1 scores between D2 and D1 blockade. Furthermore, PC1 was distinct even
377 when sessions were sorted independently and assumed to be fully statistically independent
378 (Figure S10; D2 blockade vs saline: $F = 5.8$, $p = 0.02$; D1 blockade vs saline: $F = 4.9$, $p = 0.03$;
379 all analyses accounting for variance between mice). Higher components explained less variance
380 and were not reliably different between saline and D2 blockade or D1 blockade. Taken together,
381 this data-driven analysis shows that D2 and D1 blockade produced similar shifts in MSN
382 population dynamics represented by PC1. When combined with the major contributions of
383 D1/D2 MSNs to PC1 (Fig 3C) these findings indicate that pharmacological D2 blockade and D1
384 blockade disrupt ramping-related activity in the striatum.
385
386
387

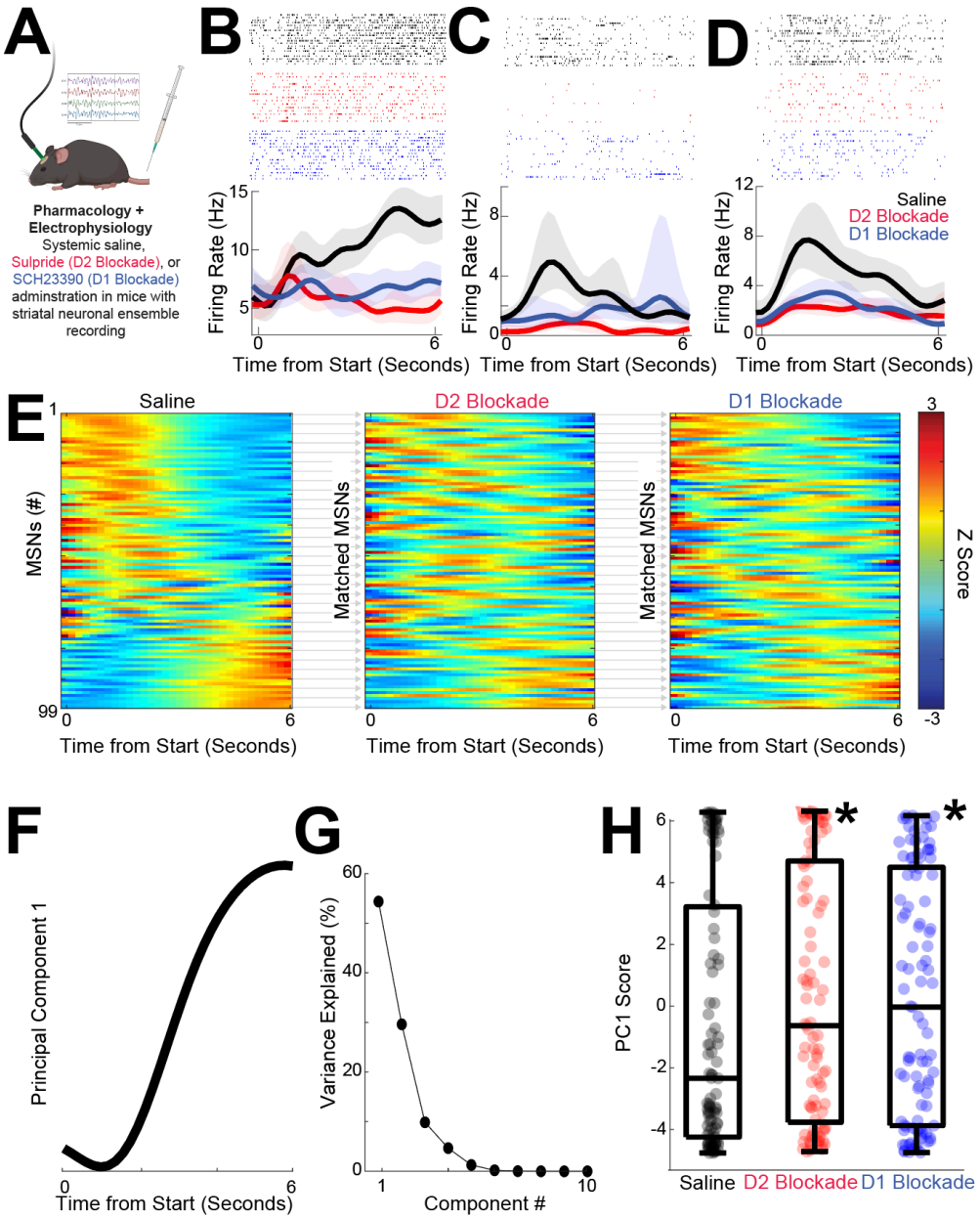

Figure 6: D2 and D1 blockade shift temporal dynamics. A) We recorded dorsomedial striatal medium spiny neuron (MSN) ensembles during interval timing in sessions with saline, D2 blockade with sulpiride, or D1 blockade with SCH23390. Made with BioRender.com. B-D) Example peri-event raster from MSNs in sessions with saline (black), D2-dopamine blockade (red), or D1-dopamine blockade (blue). Shaded area is the bootstrapped 95% confidence interval. E) MSNs from 99 neurons in 11 mice from saline, D2 blockade, or D1 blockade session; MSNs were matched across sessions based on waveforms and interspike interval. Each row represents a peri-event time histogram (PETH) binned at 0.2 seconds, smoothed using kernel-density estimates using a bandwidth of 1, and z-scored. Colors indicate z-scored firing rate. See Fig S10 for analyses that assume statistical independence. F) Principal component analysis (PCA) identified MSN ensemble patterns of activity. The first principal component (PC1) exhibited time-dependent ramping. G) PC1 explained 54% of population variance among MSN ensembles; higher components were not analyzed. H) PC1 scores were closer to zero and significantly different with D2 or D1 blockade; * = $p < 0.05$ via linear mixed effects; data from 99 MSNs in 11 mice.

389 ***D2 blockade and D1 blockade degrades MSN temporal encoding***

390 Finally, we quantified striatal MSN temporal encoding via a naïve Bayesian classifier
391 that generates trial-by-trial predictions of time from MSN ensemble firing rates (Fig 7A-C;
392 (Bruce et al., 2021; Emmons et al., 2017). Our DDMs predict that disrupted temporal decoding
393 would be a consequence of an altered DDM drift rate. We used leave-one-out cross-validation to
394 predict objective time from the firing rate within a trial. Saline sessions generated strong
395 temporal predictions for the first 6 seconds of the interval immediately after trial start (0–6
396 seconds; $R^2 = 0.91$ (0.83 – 0.94)) with weaker predictions for later epochs (6–12 seconds: $R^2 =$
397 0.55 (0.34 – 0.70); rank sum $p = 0.00002$ vs 0–6 seconds, Cohen $d = 2.0$; 12–18 seconds: $R^2 =$
398 0.18 (0.10 – 0.62); rank sum $p = 0.00003$ vs 0–6 seconds, Cohen $d = 2.4$; all analyses considered
399 each epoch statistically independent; Fig 7D). We found that temporal encoding early in the
400 interval (0–6 seconds) was degraded with either D2 blockade ($R^2 = 0.69$ (0.58 – 0.84); rank sum
401 $p = 0.0002$ vs saline, Cohen $d = 1.4$) or D1 blockade ($R^2 = 0.71$ (0.47 – 0.87); rank sum $p = 0.004$
402 vs saline, Cohen $d = 1.1$; Fig 7D), consistent with predictions made from DDMs. Later in the
403 interval (6–12 and 12-18 seconds), there were no significant differences between saline sessions
404 and D2 blockade or D1 blockade (Fig 7D).

405 Taken together, these data demonstrate that disrupting either D2-MSNs or D1-MSNs
406 degrades temporal encoding by MSN ensembles. In combination with our optogenetic tagging,
407 computational modeling, and optogenetic inhibition experiments, these data provide insight into
408 cognitive computations by the striatum.

409

410
411

412

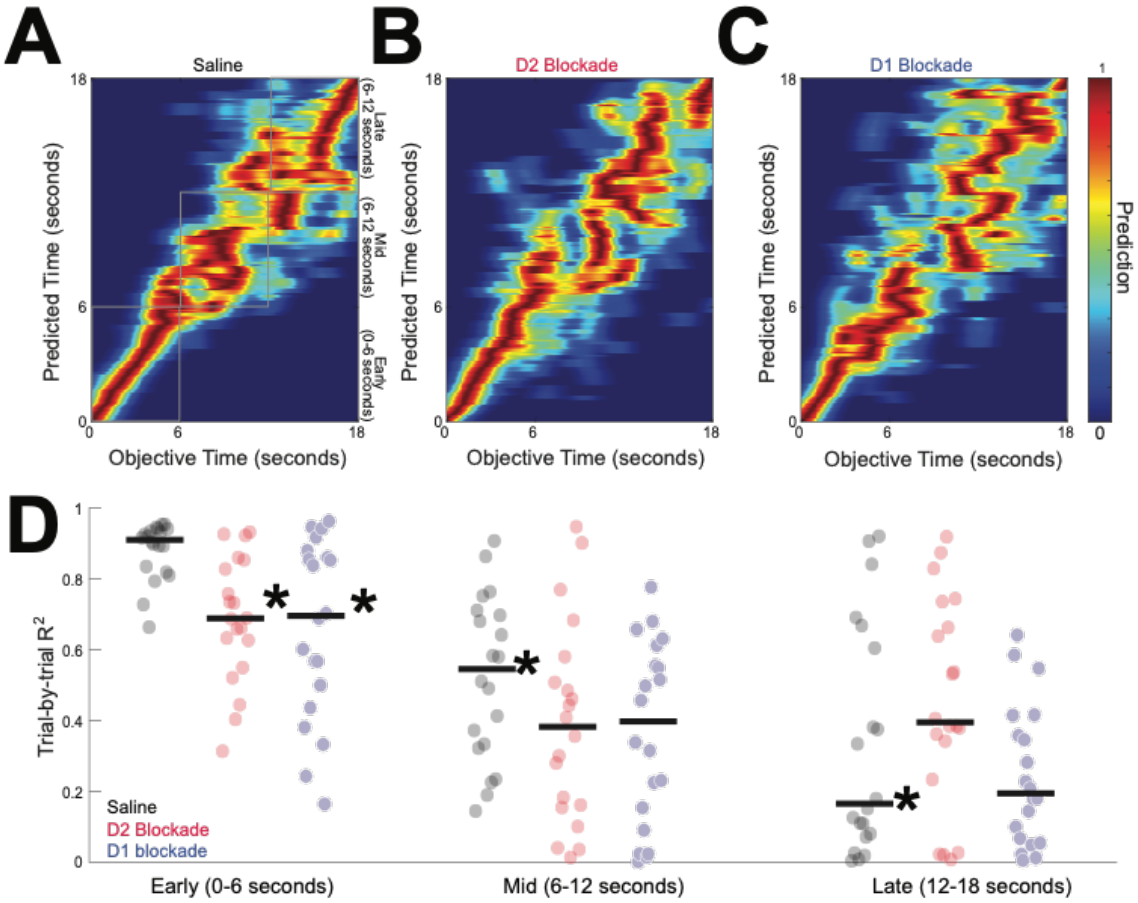

Figure 7: D2 and D1 blockade degrade MSN temporal encoding. We used naïve Bayesian classifiers to decode time from MSN ensembles in A) saline sessions, B) D2 blockade sessions, and C) D1 blockade sessions. Color represents the temporal prediction across 20 trials with red representing stronger predictions. D) Temporal encoding was strong early in the interval, and D2 or D1 blockade degraded classification accuracy. Temporal encoding was decreased later in the interval. Each point represents the R^2 for each trial of behavior for MSN ensembles from 11 mice. * $p < 0.05$ vs saline from 0-6 seconds. Horizontal black lines in (D) represent group medians.

DISCUSSION

We describe how striatal MSNs work together in complementary ways to encode an elementary cognitive process, interval timing. Strikingly, optogenetic tagging showed that D2-MSNs and D1-MSNs had distinct dynamics during interval timing. MSN dynamics helped construct and constrain a four-parameter drift-diffusion model in which D2- and D1-MSN spiking accumulated temporal evidence. This model predicted that disrupting either D2-MSNs or D1-MSNs would increase switch response times. Accordingly, we found that optogenetically or pharmacologically disrupting striatal D2-MSNs or D1-MSNs increased switch response times without affecting task-specific movements. Disrupting D2-MSNs or D1-MSNs shifted MSN temporal dynamics and degraded MSN temporal encoding. These data, when combined with our model predictions, demonstrate that D2-MSNs and D1-MSNs contribute temporal evidence to controlling actions in time. Our results provide new insight into how opposing patterns of striatal MSN activity control behavior in similar ways and show that they play a complementary role in elementary cognitive operations.

Striatal MSNs are critical for temporal control of action (Emmons et al., 2017; Gouvea et al., 2015; Mello et al., 2015). Three broad models have been proposed for how striatal MSN ensembles represent time: 1) the striatal beat frequency model, in which MSNs encode temporal information based on neuronal synchrony (Matell and Meck, 2004); 2) the distributed coding model, in which time is represented by the state of the network (Paton and Buonomano, 2018); and 3) the DDM, in which neuronal activity monotonically drifts toward a threshold after which responses are initiated (Emmons et al., 2017; Simen et al., 2011; Wang et al., 2018). While our data do not formally resolve these possibilities, our results show that D2-MSNs and D1-MSNs exhibit opposing linear changes in firing rate dynamics in PC1 over the interval. Past work by

437 our group and others has demonstrated that these linear dynamics can scale over multiple
438 intervals to represent time (Emmons et al., 2020, 2017; Gouvea et al., 2015; Mello et al., 2015;
439 Wang et al., 2018). We find that low-parameter DDMs account for interval timing behavior with
440 both intact and disrupted striatal D2- and D1-MSNs. While other models can capture interval
441 timing behavior and account for MSN neuronal activity, our model does so parsimoniously with
442 relatively few parameters (Matell and Meck, 2004; Paton and Buonomano, 2018; Simen et al.,
443 2011). We and others have shown previously that ramping activity scales to multiple intervals,
444 and DDMs can be readily adapted by changing the drift rate (Emmons et al., 2017; Gouvea et al.,
445 2015; Mello et al., 2015; Simen et al., 2011). Interestingly, decoding performance was high early
446 in the interval; indeed, animals may have been focused on this initial interval (Balci and
447 Gallistel, 2006) in making temporal comparisons and deciding whether to switch response
448 nosepokes.

449 D2-MSNs and D1-MSNs play complementary roles in movement. For instance,
450 stimulating D1-MSNs facilitates movement, whereas stimulating D2-MSNs impairs movement
451 (Kravitz et al., 2010). Both populations have been shown to have complementary patterns of
452 activity during movements (Tecuapetla et al., 2016), with MSNs firing at different phases of
453 action initiation and selection. Further dissection of action selection programs reveals that
454 opposing patterns of activation among D2-MSNs and D1-MSNs suppress and guide actions,
455 respectively, in the dorsolateral striatum (Cruz et al., 2022). A particular advantage of interval
456 timing is that it captures a cognitive behavior within a single dimension — time. When projected
457 along the temporal dimension, it was surprising that D2-MSNs and D1-MSNs had opposing
458 patterns of activity. Past pharmacological work from our group and others has shown that
459 disrupting D2- or D1-MSNs slows timing (De Corte et al., 2019b; Drew et al., 2007, 2003; Stutt

et al., 2024), in line with pharmacological and optogenetic results in this manuscript. Computational modeling predicted that disrupting either D2-MSNs or D1-MSNs increased self-reported estimates of time, which was supported by both optogenetic and pharmacological experiments. Notably, these disruptions are distinct from increased timing variability reported with administrations of amphetamine, ventral tegmental area dopamine neuron lesions, and rodent models of aging (Balci et al., 2008; Gür et al., 2020; Weber et al., 2023). Furthermore, our current data demonstrate that disrupting either D2-MSN or D1-MSN activity shifted MSN dynamics and degraded temporal encoding, supporting prior work (De Corte et al., 2019b; Drew et al., 2007, 2003; Stutt et al., 2024). Our recording experiments do not identify where a possible response threshold *T* is instantiated, but downstream basal ganglia structures may have a key role in setting response thresholds (Toda et al., 2017).

Because interval timing is reliably disrupted in human diseases of the striatum such as Huntington's disease, Parkinson's disease, and schizophrenia (Hinton et al., 2007; Singh et al., 2021; Ward et al., 2011), these results have relevance to human disease. Our task version has been used extensively to study interval timing in mice and humans (Balci et al., 2008; Bruce et al., 2021; Stutt et al., 2024; Tosun et al., 2016; Weber et al., 2023). However, temporal bisection tasks, in which animals hold during a temporal cue and respond at different locations depending on cue length, have advantages in studying how animals time an interval because animals are not moving while estimating cue duration (Paton and Buonomano, 2018; Robbe, 2023; Soares et al., 2016). Our interval timing task version – in which mice switch between two response nosepokes to indicate their interval estimate has elapsed – has been used extensively in rodent models of neurodegenerative disease (Larson et al., 2022; Weber et al., 2024, 2023; Zhang et al., 2021), as well as in humans (Stutt et al., 2024). Furthermore, because many therapeutics targeting

483 dopamine receptors are used clinically, these findings help describe how dopaminergic drugs
484 might affect cognitive function and dysfunction. Future studies of D2-MSNs and D1-MSNs in
485 temporal bisection and other timing tasks may further clarify the relative roles of D2- and D1-
486 MSNs in interval timing and time estimation.

487 Our approach has several limitations. First, systemic drug injections block D2- and D1-
488 receptors in many different brain regions, including the frontal cortex, which is involved in
489 interval timing (Kim et al., 2017a). D2 blockade or D1 blockade may have complex effects,
490 including corticostriatal or network effects that contribute to changes in D2-MSN or D1-MSN
491 ensemble activity. We note that optogenetic inhibition of D2-MSNs and D1-MSNs produces
492 similar effects to pharmacology in Figure 5. Pharmacology is compatible with neuronal
493 ensemble recordings as optogenetic inhibition would silence a large fraction of neurons,
494 complicating interpretations. Future studies might extend our work by combining local
495 pharmacology with neuronal ensemble recording. Second, although we had adequate statistical
496 power and medium-to-large effect sizes, optogenetic tagging is low-yield, and it is possible that
497 recording more of these neurons would afford greater opportunity to identify more robust results
498 and alternative coding schemes, such as neuronal synchrony. Furthermore, we find that recording
499 more neurons simultaneously would also help further constrain DDMs to predict trial-by-trial
500 firing rate and generate a more sophisticated neuronal network model of time (Fig S4). Third, the
501 striatum includes diverse cell types, some of which express both D1 and D2 dopamine receptors;
502 these cell types may also contribute to cognitive processing. Fourth, MSNs can laterally inhibit
503 each other, which may profoundly affect striatal function. Regardless, we show that cell-type-
504 specific disruption of D2-MSNs and D1-MSNs both slow timing, implying that these cell types
505 play a key role in interval timing. Future experiments may record from non-MSN striatal cell

types, including fast-spiking interneurons that shape basal ganglia output. Fifth, we did not deliver stimulation to the striatum because our pilot experiments triggered movement artifacts or task-specific dyskinesias (Kravitz et al., 2010). Future stimulation approaches carefully titrated to striatal physiology may affect interval timing without affecting movement. Finally, movement and motivation contribute to MSN dynamics (Robbe, 2023). Four lines of evidence argue that our findings cannot be directly explained by motor confounds: 1) D2-MSNs and D1-MSNs diverge between 0-6 seconds after trial start well before the first nosepoke (Fig S2), 2) our GLM accounted for nosepokes and nosepoke-related βs were similar between D2-MSNs and D1-MSNs, 3) optogenetic disruption of dorsomedial D2-MSNs and D1-MSNs did not change task-specific movements despite reliable changes in switch response time, and 4) ramping dynamics were quite distinct from movement dynamics. Furthermore, disrupting D2-MSNs and D1-MSNs did not change the number of rewards animals received, implying that these disruptions did not grossly affect motivation. Still, future work combining motion tracking with neuronal ensemble recording and optogenetics and including bisection tasks may further unravel timing vs. movement in MSN dynamics (Robbe, 2023).

In summary, we examined the role of dorsomedial striatal D2-MSNs and D1-MSNs during an elementary cognitive behavior, interval timing. Optogenetic tagging revealed that D2-MSNs and D1-MSNs exhibited opposite and complementary patterns of neuronal activity. These dynamics could be captured by computational drift-diffusion models, which predicted that disrupting either D2-MSNs or D1-MSNs would slow the accumulation of temporal evidence and increase switch response time. In line with this prediction, we found that optogenetic or pharmacological disruption of either D2-MSNs or D1-MSNs increased switch response times, with pharmacological D2 or D1 blockade shifting MSN dynamics and degrading temporal

529 decoding. Collectively, our data provide insight into how the striatum encodes cognitive
530 information, which could be highly relevant for human diseases that disrupt the striatum and for
531 next-generation neuromodulation that targets the basal ganglia to avoid cognitive side effects or
532 to treat cognitive dysfunction.
533

534 **Methods and Materials**

535 ***Rodents.*** All procedures were approved by the Institutional Animal Care and Use Committee
536 (IACUC) at the University of Iowa, and all experimental methods were performed in accordance
537 with applicable guidelines and regulations (Protocol #0062039). We used five cohorts of mice,
538 summarized in Table 1: 1) 30 wild-type C57BL/6J mice (17 female) for behavioral experiments
539 (Fig 1), 2) 4 *Drd2-cre*+ mice derived from Gensat strain ER44 (2 female) and 5 *Drd1-cre*+ mice
540 derived from Gensat strain EY262 (2 female) for optogenetic tagging and neuronal ensemble
541 recordings in Fig 2-3; 3) 10 *Drd2-cre*+ (5 female), and 6 *Drd1-cre*+ mice (3 female) for
542 optogenetic inhibition (Fig 5) with 5 *Drd2-cre*+ and 5 *Drd1-cre*+ controls and 4) 10 wild-type
543 mice for behavioral pharmacology (Fig 5), and 5) 11 mice (4 C57BL/6J (2 female), 5 *Drd2-cre*+
544 mice (2 female), and 2 *Drd1-cre*+ mice (0 female)) for combined behavioral pharmacology and
545 neuronal ensemble recording (Fig 6-7) (Table 1). Our recent work shows that D2-blockade and
546 D1-blockade have similar effects in both sexes(Stutt et al., 2024).

547 ***Interval timing switch task.*** We used a mouse-optimized operant interval timing task described
548 in detail previously (Balci et al., 2008; Bruce et al., 2021; Tosun et al., 2016; Weber et al., 2023).
549 Briefly, mice were trained in sound-attenuating operant chambers, with two front nosepokes
550 flanking either side of a food hopper on the front wall, and a third nosepoke located at the center
551 of the back wall. The chamber was positioned below an 8-kHz, 72-dB speaker (Fig 1A;
552 MedAssociates, St. Albans, VT). Mice were 85% food restricted and motivated with 20 mg
553 sucrose pellets (Bio-Serv, Flemington, NJ). Mice were initially trained to receive rewards during
554 fixed ratio nosepoke response trials. Nosepoke entry and exit were captured by infrared beams.
555 After shaping, mice were trained in the "switch" interval timing task. Mice self-initiated trials at

556 the back nosepoke, after which tone and nosepoke lights were illuminated simultaneously. Cues
557 were identical on all trial types and lasted the entire duration of the trial (6 or 18 seconds). On
558 50% of trials, mice were rewarded for a nosepoke after 6 seconds at the designated first 'front'
559 nosepoke; these trials were not analyzed. On the remaining 50% of trials, mice were rewarded
560 for nosepoking first at the 'first' nosepoke location and then switching to the 'second' nosepoke
561 location; the reward was delivered for initial nosepokes at the second nosepoke location after 18
562 seconds when preceded by a nosepoke at the first nosepoke location. Multiple nosepokes at each
563 nosepokes were allowed. Early responses at the first or second nosepoke were not reinforced.
564 Initial responses at the second nosepoke rather than the first nosepoke, alternating between
565 nosepokes, going back to the first nosepoke after the second nosepoke were rare after initial
566 training. Error trials included trials where animals responded only at the first or second nosepoke
567 and were also not reinforced. We did not analyze error trials as they were often too few to
568 analyze; these were analyzed at length in our prior work (Bruce et al., 2021).

569 *Switch response time* was defined as the moment animals departed the first nosepoke
570 before arriving at the second nosepoke. Critically, switch responses are a time-based decision
571 guided by temporal control of action because mice switch nosepokes only if nosepokes at the
572 first location did not receive a reward after 6 seconds. That is, mice estimate if more than 6
573 seconds have elapsed without receiving a reward to decide to switch responses. Mice learn this
574 task quickly (3-4 weeks), and error trials in which an animal nosepokes in the wrong order or
575 does not nosepoke are relatively rare and discarded. Consequently, we focused on these switch
576 response times as the key metric for temporal control of action. *Traversal time* was defined as
577 the duration between first nosepoke exit and second nosepoke entry and is distinct from switch
578 response time when animals departed the first nosepoke. *Nosepoke duration* was defined as the

579 time between first nosepoke entry and exit for the switch response times only. Trials were self-
580 initiated, but there was an intertrial interval with a geometric mean of 30 seconds between trials.

581 ***Surgical and histological procedures.*** Surgical procedures were identical to methods described
582 previously (Bruce et al., 2021). Briefly, mice were anesthetized using inhaled 4% isoflurane and
583 surgical levels of anesthesia were maintained at 1-2% for the duration of the surgery.
584 Craniotomies were drilled above bilateral dorsal striatal anatomical targets, and optogenetic
585 viruses (AAV5-DIO-eNHPR2.0 (halorhodopsin), AAV5-DIO-ChR2(H134R)-mcherry (ChR2),
586 or AAV5-DIO-cherry (control) from the University of North Carolina Viral Vector Core) were
587 injected into the dorsal striatum (0.5 uL of virus, +0.9, ML +/-1.3, DV –2.7). Either fiber optics
588 (Doric Lenses, Montreal Quebec; AP +0.9, ML +/-1.3, DV –2.5) or 4 x 4 electrode or optrode
589 arrays (AP +0.4, ML -1.4, DV -2.7 on the left side only; Microprobes, Gaithersburg, MD) were
590 positioned in the dorsal striatum. Holes were drilled to insert skull screws to anchor headcap
591 assemblies and/or ground electrode arrays and then sealed with cyanoacrylate ("SloZap," Pacer
592 Technologies, Rancho Cucamonga, CA), accelerated by "ZipKicker" (Pacer Technologies) and
593 methyl methacrylate (AM Systems, Port Angeles, WA). Following postoperative recovery, mice
594 were trained on the switch task and acclimated to experimental procedures prior to undergoing
595 experimental sessions.

596 ***Optogenetics.*** We leveraged cell-type-specific optogenetics to manipulate D2-MSNs and D1-
597 MSNs in D2-cre or D1-cre mice. In animals injected with optogenetic viruses, optical inhibition
598 was delivered via bilateral patch cables for the entire trial duration of 18 seconds via 589-nm
599 laser light at 12 mW power on 50% of randomly assigned trials. We performed control
600 experiments in mice without opsins using identical laser parameters in D2-cre or D1-cre mice

601 (Fig S6). We did not stimulate for epochs less than the interval because we did not want to
602 introduce a cue during the interval. For optogenetic tagging, putative D1- and D2-MSNs were
603 optically identified via 473-nm photostimulation. Units with mean post-stimulation spike
604 latencies of ≤5 milliseconds and a stimulated-to-unstimulated waveform correlation ratio of >0.9
605 were classified as putative D2-MSNs or D1-MSNs (Ryan et al., 2018; Shin et al., 2018). Only
606 one recording session was performed for each animal per day, and one recording session was
607 included from each animal.

608 ***Behavioral pharmacology procedures.*** C57BL/6J mice were injected intraperitoneally (IP) 20-
609 40 minutes before interval timing trials with either SCH23390 ($C_{17}H_{18}ClNO$; D1 antagonist),
610 sulpiride ($C_{15}H_{23}N_3O_4S$; D2 antagonist), or isotonic saline. The sulpiride dosage was 12.5 mg/kg,
611 0.01 mL/g, and the SCH23390 was administered at a dosage of 0.05 mg/kg, 0.01 mL/g.
612 Behavioral performance was compared with interval timing behavior on the prior day when
613 isotonic saline was injected IP. Only one recording session was performed for each animal per
614 day, and one recording session was included from saline, D2 blockade, and D1 blockade
615 sessions.

616 ***Electrophysiology.*** Single-unit recordings were made using a multi-electrode recording system
617 (Open Ephys, Atlanta, GA). After the experiments, Plexon Offline Sorter (Plexon, Dallas, TX),
618 was used to remove artifacts. Principal component analysis (PCA) and waveform shape were
619 used for spike sorting. Single units were defined as those 1) having a consistent waveform shape,
620 2) being a separable cluster in PCA space, and 3) having a consistent refractory period of at least
621 2 milliseconds in interspike interval histograms. The same MSNs were sorted across saline, D2
622 blockade, and D1 blockade sessions by loading all sessions simultaneously in Offline Sorter and

623 sorted using the preceding criteria. MSNs had to have consistent firing in all sessions to be
624 included. Sorting integrity across sessions was quantified by comparing waveform similarity via
625 correlation coefficients between sessions.

626 Spike activity was analyzed for all cells that fired between 0.5 Hz and 20 Hz over the
627 entire behavioral session. Putative MSNs were further separated from striatal fast-spiking
628 interneurons (FSIs) based on hierarchical clustering of the waveform peak-to-trough ratio and the
629 half-peak width (*fitgmdist* and *cluster.m*; Fig S1; (Berke, 2011)). We calculated kernel density
630 estimates of firing rates across the interval (-4 seconds before trial start to 22 seconds after trial
631 start) binned at 0.2 seconds, with a bandwidth of 1. We used PCA to identify data-driven patterns
632 of z-scored neuronal activity, as in our past work (Bruce et al., 2021; Emmons et al., 2017; Kim
633 et al., 2017a). The variance of PC1 was empirically compared against data generated from 1000
634 iterations of data from random timestamps with identical bins and kernel density estimates.
635 Average plots were shown with Gaussian smoothing for plotting purposes only.

636 ***Immunohistochemistry.*** Following completion of experiments, mice were transcardially
637 perfused with ice-cold 1x phosphate-buffered saline (PBS) and 4% paraformaldehyde (PFA)
638 after anesthesia using ketamine (100 mg/kg IP) and xylazine (10 mg/kg IP). Brains were then
639 fixed in solutions of 4% PFA and 30% sucrose before being cryosectioned on a freezing
640 microtome. Sections were stained for tyrosine hydroxylase with primary antibodies for >12
641 hours (rabbit anti-TH; Millipore MAB152; 1:1000) at 4° C. Sections were subsequently
642 visualized with Alexa Fluor fluorescent secondary antibodies (goat anti-rabbit IgG Alexa 519;
643 Thermo Fisher Scientific; 1:1,000) matched to host primary by incubating 2 hours at room
644 temperature. Histological reconstruction was completed using postmortem analysis of electrode

645 placement by slide-scanning microscopy on an Olympus VS120 microscope (Olympus, Center
646 Valley, PA; Fig S2&S4).

647 ***Trial-by-trial GLMs.*** To measure time-related ramping over the first 6 seconds of the interval,
648 we used trial-by-trial generalized linear models (GLMs) at the individual neuron level in which
649 the response variable was firing rate and the predictor variable was time in the interval or
650 nosepoke rate (Shimazaki and Shinomoto, 2007). For each neuron, its time-related "ramping"
651 slope was derived from the GLM fit of firing rate vs time in the interval, for all trials per neuron.
652 GLMs accounted for nosepoke movements unless there were no nosepokes within the 0-6 second
653 interval. All GLMs were run at a trial-by-trial level to avoid the effects of trial averaging
654 (Latimer et al., 2015) as in our past work (Bruce et al., 2021; Emmons et al., 2017; Kim et al.,
655 2017b). We performed additional sensitivity analyses excluding outliers outside of 95%
656 confidence intervals and measuring the firing rate from the start of the interval to the time of the
657 switch response on a trial-by-trial level for each neuron.

658 ***Machine-learning analyses***. To predict time, we used a naïve Bayesian classifier to evaluate
659 neuronal ensemble decoding as in our past work (Emmons et al., 2020, 2017; Gouvea et al.,
660 2015; Kim et al., 2017a; Mello et al., 2015). Data from neurons with more than 20 trials across
661 all mice with the goal of evaluating how the decoding of time is affected by the epoch in the
662 interval and by D2/D1 blockade. To preclude edge effects that might bias classifier performance,
663 we included data from 6 seconds before trial start and 6 seconds after the end of the interval. We
664 used leave-one-out cross-validation to predict an objective time from the firing rate within a trial.
665 Classifier performance was quantified by computing the R^2 of objective time vs predicted time,

only for bins during the interval (0-6, 6-12, and 12-18 seconds; see Fig 7). Classifier performance was compared using time-shuffled firing rates via a Wilcoxon signed-rank test.

Drift-diffusion models (DDM). We constructed a four-parameter DDM (see Equations 1-3 in Results) that accounted for the ensemble threshold behavior observed in the neural data, then used it to simulate switch response times compatible with mice behavioral data. The model was implemented in MATLAB, starting from initial value b and with discrete computer simulation steps $x_{new} = x_{old} + (F - x_{old})D\Delta t + \sigma\sqrt{\Delta t}N(0,1)$. Here $N(0,1)$ represents random values generated from the standardized Gaussian distribution (mean = 0 and standard deviation = 1). The integration timestep was $\Delta t = 0.1$. For each numerical simulation, the "switch response time" was defined as the time t^* when variable x first reached the threshold value $T = F(1 - b/4) + (1 - F)b/4$. For each condition, we ran 500 simulations of the model (up to 25 seconds per trial) and recorded the switch response times. Examples of firing rate x dynamics are shown in Fig 4A-B. We observed that the distributions of interval timing switch response times could be fit by a gamma probability distribution function $PDF(x) = \frac{\beta^\alpha}{\Gamma(\alpha)}\, x^{\alpha-1}\, e^{-\beta x}$ with shape α and rate β (see Fig S7 and Table S2).

Analysis and modeling of mouse MSN-ensemble recordings. Our preliminary analysis found that, for sufficiently large number of neurons ($N > 11$), each recorded ensemble of MSNs on a trial-by-trial basis could predict when mice would respond. We took the following approach: *First*, for each MSN, we convolved its trial-by-trial spike train $Spk(t)$ with a 1-second exponential kernel $K(t) = w\, e^{-t/w}$ if $t > 0$ and $K(t) = 0$ if $t \leq 0$ (Zhou et al., 2018; here $w = 1\ s$). Therefore, the smoothed, convolved spiking activity of neuron j ($j = 1,2, \ldots N$),

$$x_j(t) = \left(Spk_j * K\right)(t) = \int_{-\infty}^{\infty} K(s) Spk_j(t-s)ds = \int_{0}^{\infty} K(s) Spk_j(t-s)ds$$

tracks and accumulates the most recent (one second, in average) firing-rate history of the j-th MSN, up to moment t. We hypothesized that the ensemble activity $(x_1(t), x_2(t), \dots, x_N(t))$, weighted with some weights β_j , could predict the trial switch time t^* by considering the sum

$$x(t) = \sum_{j=1}^{N} \beta_j \, x_j(t)$$

and the sigmoid

$$y(t) = \frac{1}{1 + \exp\left(-(x(t) - 0.5)/k\right)} = \frac{1}{1 + \exp\left[-\left(\hat{\beta}_0 + \sum_{j=1}^{N} \hat{\beta}_j x_j(t)\right)\right]}$$

that approximates the firing rate of an output unit. Here parameter k indicates how fast $x(t)$ crosses the threshold 0.5 coming from below (if $k > 0$) or coming from above (if $k < 0$) and relates the weights β_j to the unknowns $\hat{\beta}_j = \beta_j/k$ and $\hat{\beta}_0 = -0.5/k$. Next, we ran a logistic fit for every trial for a given mouse over the spike count predictor matrix $\left(x_1(t), x_2(t), \dots, x_N(t)\right)$ from the mouse MSN recorded ensemble, and observed value t^*, estimating the coefficients $\hat{\beta}_0$ and $\hat{\beta}_j$, and so, implicitly, the weights β_j. From there, we compute the predicted switch time t^*_{pred} by condition $x(t) = 0.5$. Accuracy was quantified comparing the predicted accuracy within a 1 second window to switch time on a trial-by-trial basis (Fig S4).

Statistics. All data and statistical approaches were reviewed by the Biostatistics, Epidemiology, and Research Design Core (BERD) at the Institute for Clinical and Translational Sciences

705 (ICTS) at the University of Iowa. All code and data are made available at
706 http://narayanan.lab.uiowa.edu/article/datasets. We used the median to measure central tendency
707 and the interquartile range to measure spread. We used Wilcoxon nonparametric tests to compare
708 behavior between experimental conditions and Cohen's *d* to calculate effect size. Analyses of
709 putative single-unit activity and basic physiological properties were carried out using custom
710 routines for MATLAB.

711 For all neuronal analyses, variability between animals was accounted for using
712 generalized linear-mixed effects models and incorporating a random effect for each mouse into
713 the model, which allows us to account for inherent between-mouse variability. We used *fitglme*
714 in MATLAB and verified main effects using *lmer* in R. We accounted for variability between
715 MSNs in pharmacological datasets in which we could match MSNs between saline, D2
716 blockade, and D1 blockade. P values < 0.05 were interpreted as significant.

717

Data Availability

All raw data are available at http://narayanan.lab.uiowa.edu/article/datasets.

Code Availability

All code is available at http://narayanan.lab.uiowa.edu/article/datasets.

Acknowledgements

This work was funded by NIMH R01MH116043 to NSN. We thank Bernardo Sabatini for detailed feedback on our manuscript.

Author Contributions

RAB, MAW, and NN designed the experiments. RAB, MAW, ASB, RV, CJ, and HRS performed all experiments and collected data. The data was analyzed by RAB, MAW, ASB, HRS, YK, RC, and NN. RC developed the computational model. RAB, MAW, ASB, KS, RC, and NN wrote the manuscript, and all authors reviewed and revised the manuscript.

Table 1: Summary of mice, sessions, # of switch trials, and MSNs

Experiment	Figure	Cohort	Mice	# Sessions median (Q1-Q3)	# of Switch Responses	Neurons
Interval timing behavior	Fig 1B-C	1	30 wild-type mice	2 (2-2)	34 (25-42)	~
Optogenetic Tagging of D2-MSNs	Fig 2-3	2	4 D2-Cre mice	1 (1-1)	25 (22-25)	32 D2-MSNs
Optogenetic Tagging of D1-MSNs	Fig 2-3		5 D1-Cre mice	1(1-1)	22 (10-28)	41 D1-MSNs
Drift-diffusion models (DDM)	Fig 4A-D, Fig S4&S7	N/A	N/A	N/A	N/A	N/A
Optogenetic Inhibition of D2-MSNs	Fig 5A-B	3	10 D2-Cre mice	6(4-8)	127(78-135)	~
Optogenetic Inhibition of D1-MSNs	Fig 5C-D		6 D1-Cre mice	6(4-8)	81(60-106)	~
Optogenetic D2-MSN controls	Fig S7		5 D2-Cre mice	6(4-7)	104(60-140)	~
Optogenetic D1-MSN controls	Fig S7		5 D1-Cre mice	7(4-7)	102(78-128)	~
Pharmacological D2 blockade	Fig 5E-F	4	10 wild-type mice	2(2-2)	28(17-36)	~
Pharmacological D1 blockade	Fig 5G-H			2(2-2)	29(25-30)	~
MSN ensemble recording - saline	Fig 6-7, Fig S10	5	4 wild-type mice 5 D2-cre mice, and 2 D1-cre mice	1(1-1)	23(21-30)	158 MSNs
MSN ensembles – D2 blockade	Fig 6-7, Fig S10			1(1-1)	15(11-22)	167 MSNs
MSN ensembles – D1 blockade	Fig 6-7, Fig S10			1(1-1)	16(13-26)	144 MSNs

Supplementary Information

Condition	***Source***	***α***	***β***	
D2-MSNs Laser Off	Empirical Data	6.03	0.67	Fig S7A
D2-MSNs Laser Off	Model	6.08	0.69	Fig S7E
D2-MSNs Inhibited	Empirical Data	7.62	0.78	Fig S7B
D2-MSNs Inhibited	Model	7.67	0.79	Fig S7F
D1-MSNs Laser Off	Empirical Data	5.87	0.68	Fig S7C
D1-MSNs Laser Off	Model	5.89	0.69	Fig S7G
D1-MSNs Inhibited	Empirical Data	7.13	0.70	Fig S7D
D1-MSNs Inhibited	Model	7.31	0.72	Fig S7H

Table S2: Gamma distribution parameters

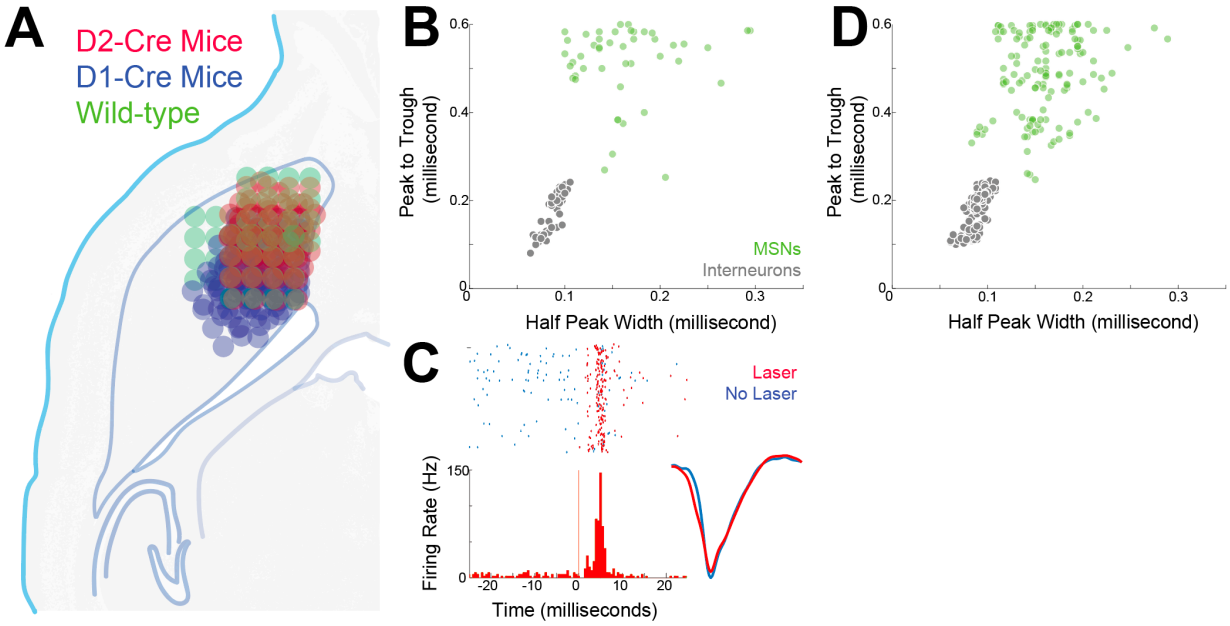

Figure S1: A) Recording locations in the dorsomedial striatum (targeting AP +0.4, ML -1.4, DV -2.7). Electrode reconstructions for D2-Cre (red), D1-Cre (blue), and wild-type mice (green). Only the left striatum was implanted with electrodes in all animals. B) MSN classification by waveform criteria for sessions with optogenetic tagging. C) Example of an optogenetically tagged MSN. This neuron expresses ChR2 and fired action potentials within 5 milliseconds of 473 nm laser pulses (red line). Spikes from laser trials shown as red ticks; trials without laser shown as blue ticks. Inset on bottom right – waveforms from laser trials (red) and trials without laser (blue). Across 73 tagged neurons, waveform correlation coefficients for laser trials vs. trials without laser was r = 0.97 (0.92-0.99), indicating that optogenetically triggered spikes were similar to non-optogenetically triggered spikes. D) MSN classification by waveform criteria for pharmacology sessions.

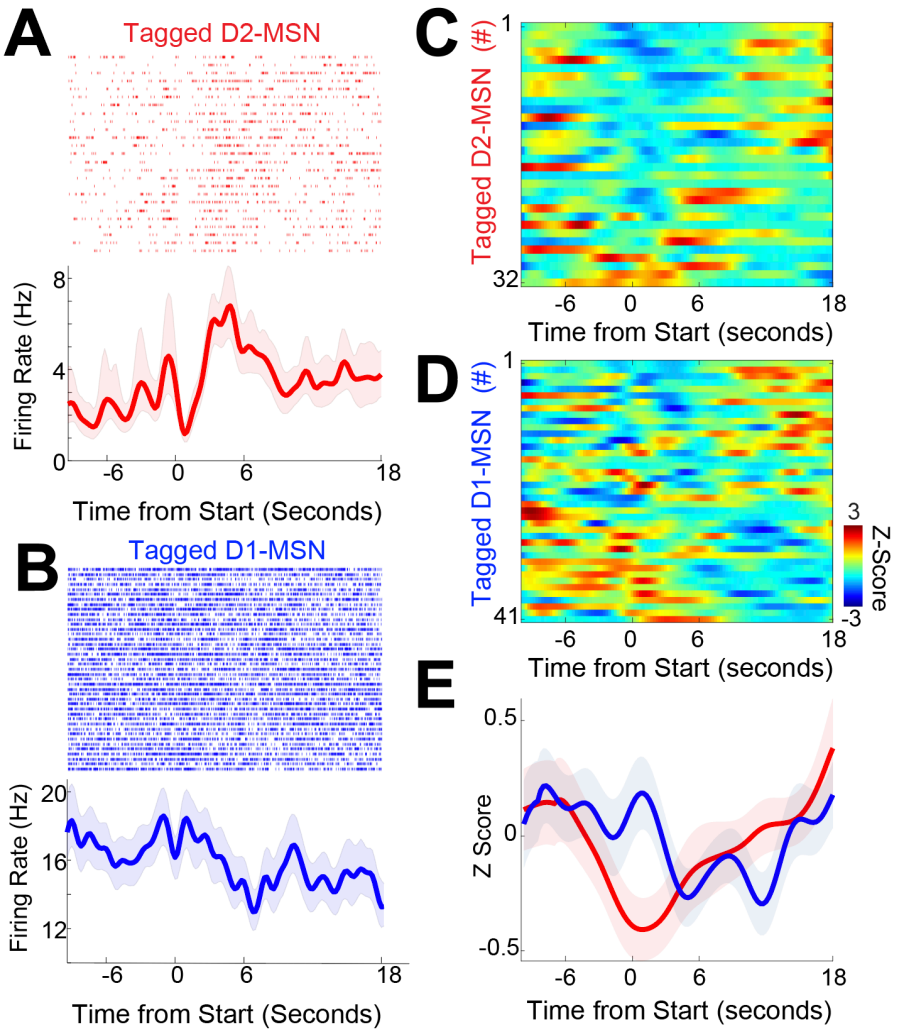

Figure S2: D2- and D1-MSN activity over a longer epoch from 10 seconds prior to trial start, when mice initiated trials at the back nosepoke, to the end of 18 seconds, after which making a second nosepoke led to reward. A) Tagged D2-MSN from Figure 2C shown over a longer interval, and B) tagged D1-MSN from Figure 2D shown over a longer interval. C) Peri-event time histograms from D2-MSNs and D) from D1-MSNs over a longer interval. E) We noticed that on average, D2-MSNs and D1-MSNs had the biggest differences in dynamics, where they tended to have distinct slopes (Fig 3C&D); slope analyses were less reliable for other epochs. Data from 32 tagged D2-MSNs in 4 D2-Cre mice and 41 tagged D1-MSNs in 5 D1-Cre mice as in Fig 2.

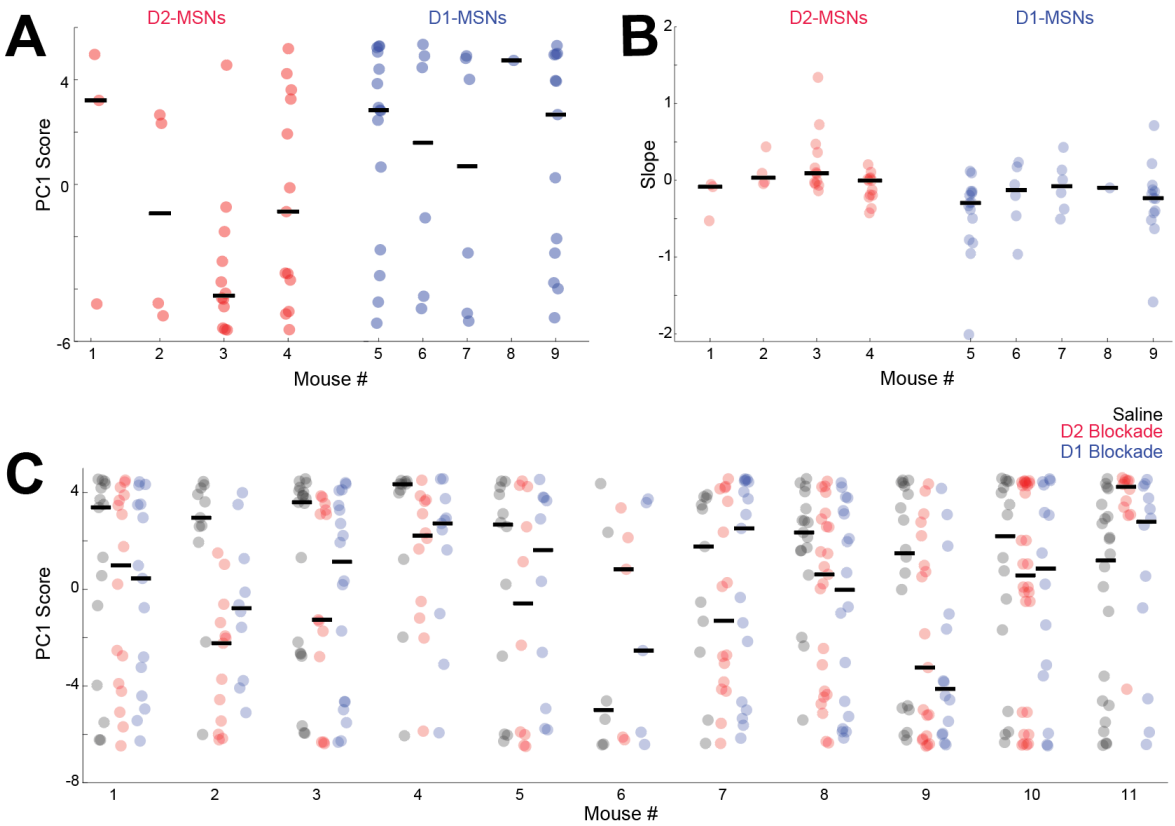

Figure S3: Effects in individual mice from optogenetic tagging experiments for A) PC1 and B) trial-by-trial GLM slope of firing rate over the interval; red = D2-MSN, and blue = D1-MSN. C) Effects in individual mice for PC1 for all neurons from combined pharmacology and neuronal ensemble recording; black is saline, red is D2 Blockade, and blue is D1 Blockade. Black lines indicate the median for each condition in each mouse. All statistics analyzing these data used linear-mixed effects models as incorporating a random effect for each mouse into the model allows to account for inherent between-mouse variability.

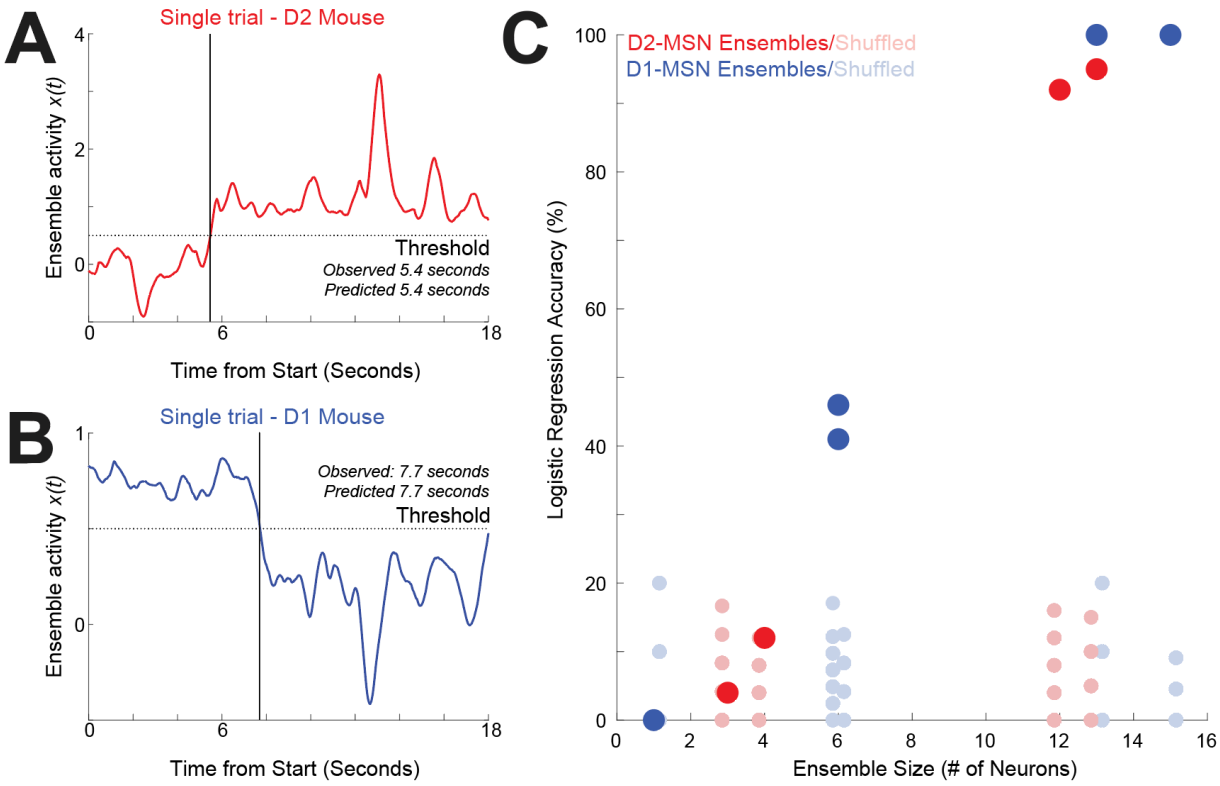

Figure S4: Trial-by-trial predictions of switch response time from D2-MSN and D1-MSN ensemble dynamics. A) Exemplar integral of network activity $x(t) = \sum \beta_j x_j(t)$ generated from an ensemble of 13 D2-MSNs for a single animal on a single trial. The coefficients β_j were computed from the logistic regression fit to the switch time t^* using the neurons firing rates $(x_j(t))_j$ as the predictor matrix (see Methods). On this trial, this integral drifted towards the response threshold 0.5, and logistic regression accurately predicted the switch response time. B) Exemplar integral network activity $x(t)$ generated from an ensemble of 15 D1-MSNs in a single animal on a single trial. C) Across all D2-MSN and D1-MSN ensembles per individual mouse, we found that the trial-by-trial accuracy increased with ensemble size, exceeding >90% when D2-MSN and D1-MSN ensembles were >11 neurons. Neuronal data from 5 D1-Cre (blue dots) and 4 D2-Cre (red dots) mice in Figures 2-3. Corresponding light blue/light red dots show accuracy values computed in 100 simulations of respective D2-MSN/D1-MSN ensembles with Poisson spikes matched to MSN firing rates.

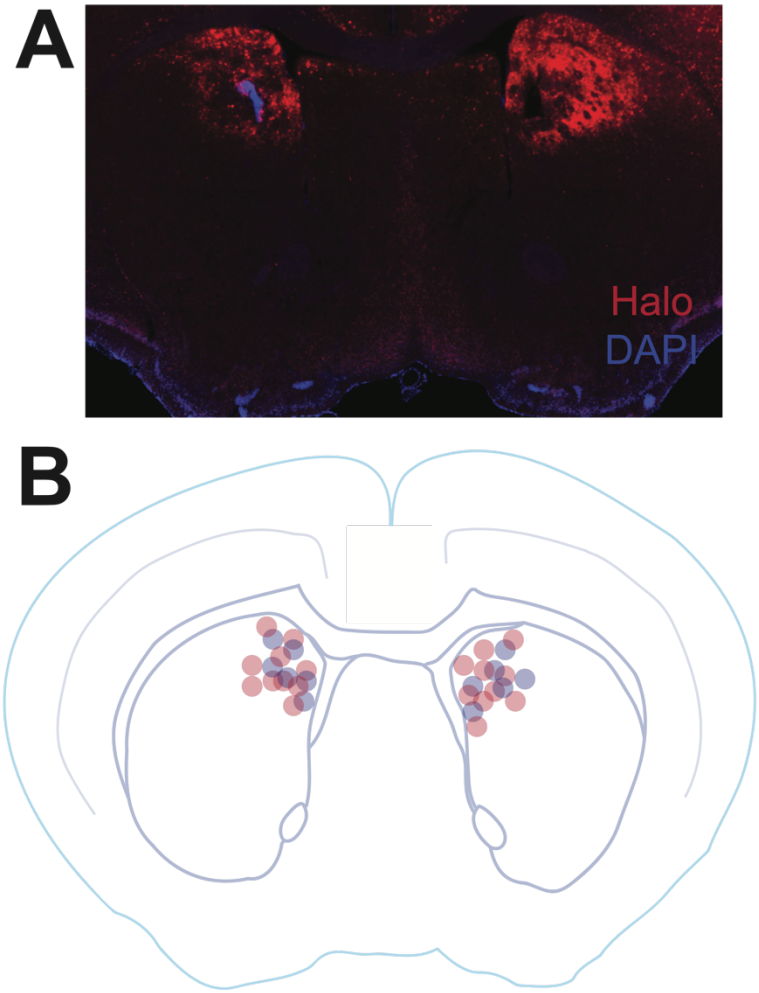

Figure S5: Fiber optic locations from A) an opsin-expressing mouse with mCherry-tagged halorhodopsin and bilateral fiber optics, and B) across 10 D2-Cre mice (red) and 6 D1-cre mice (blue) with fiber optics (targeting AP +0.9, ML +/-1.3, DV –2.5).

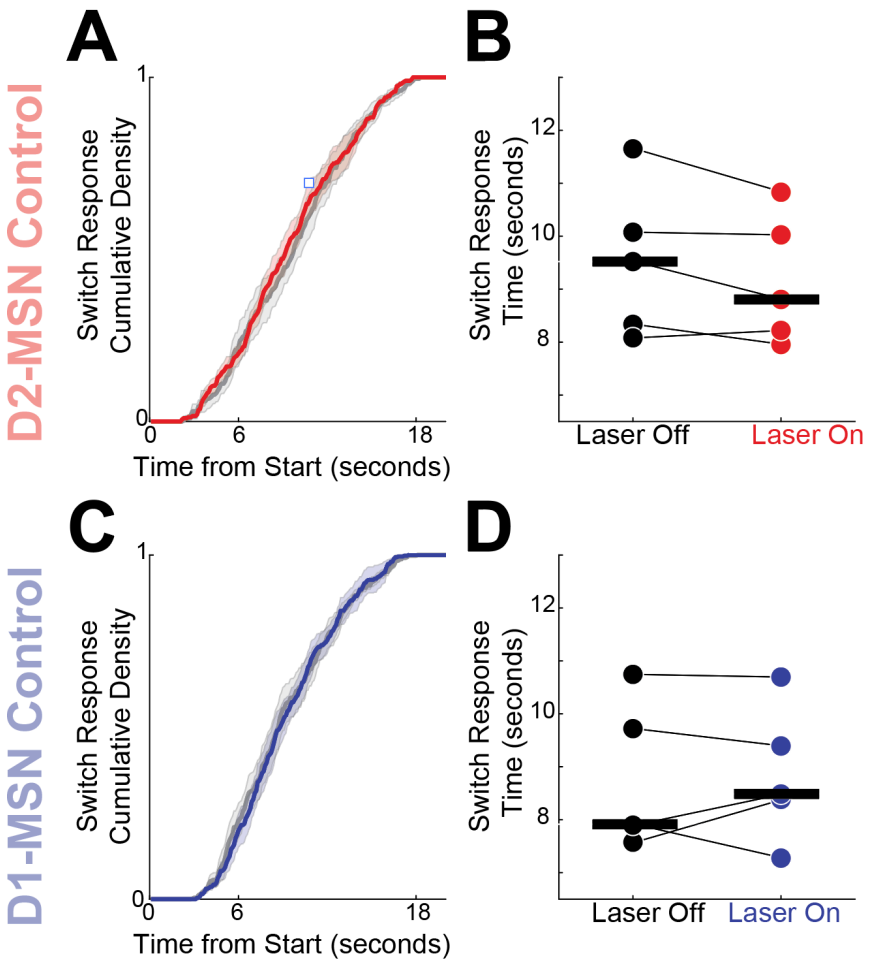

806

807 **Figure S6**: Experiments in D2-Cre mice injected with virus without opsins did not reliably affect

808 A) cumulative density functions (CDFs) or B) switch response times (signed rank $p = 0.44$).

809 Experiments in D1-Cre mice expressing virus without opsins did not reliably affect C) CDFs or

810 D) switch response times (signed rank $p = 0.81$). Laser parameters (589 nm laser, 12 mW, 18

811 second duration) were identical to experimental animals in Fig 5.

812

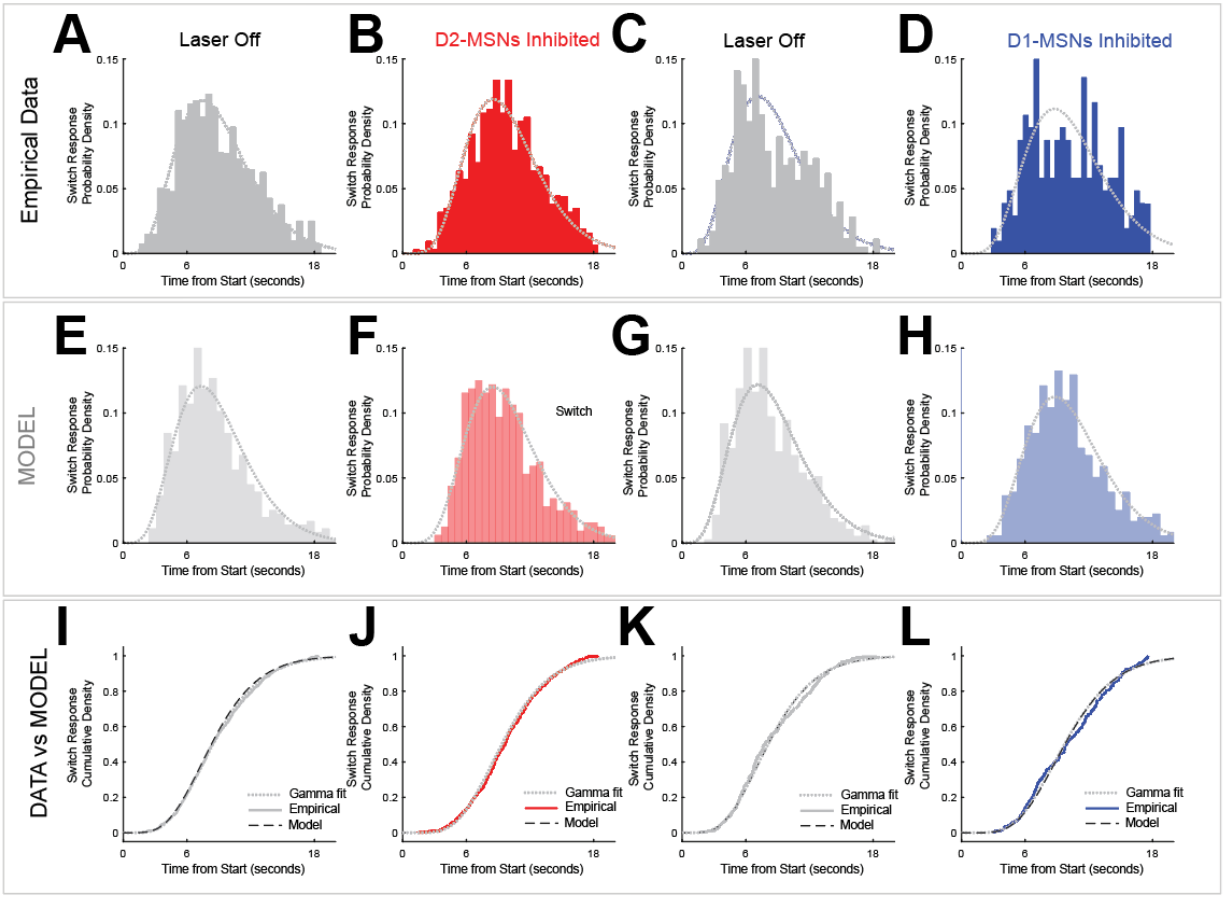

Figure S7: Model details. Histograms of behavioral data from D2-Cre mice with A) Laser Off and B) D2-MSN inhibition (red). Data from D1-Cre mice with C) Laser Off and with D) D1-MSN inhibition (blue). E-H) model predictions. I-L) Comparisons of empirical data vs model. All panels: fits for the gamma distribution with dotted circles; see Table S2 for the parameter values defining each gamma distribution. Behavioral data: from 10 D2-Cre mice and 6 D1-mice from Fig 5A-D. Model data: from numerical simulations of the DDM model shown in Fig 4. All DDM parameters were chosen to fit behavioral data in each condition.

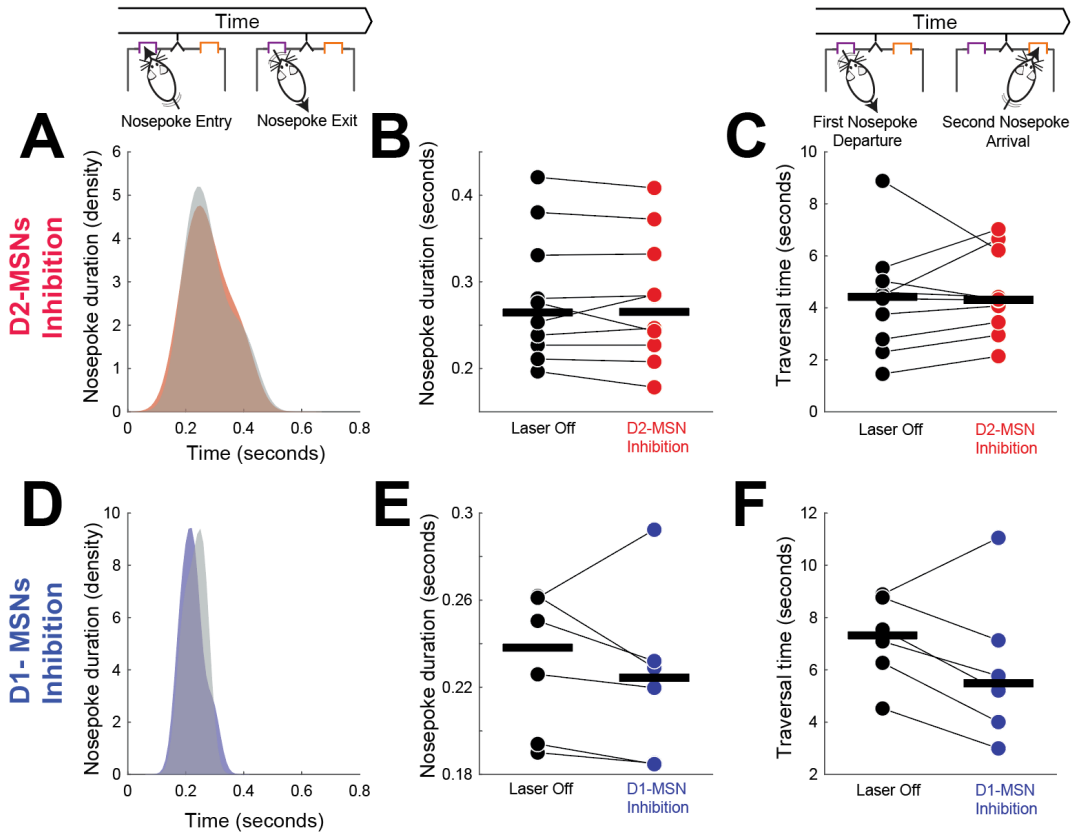

Figure S8: Optogenetically inhibiting D2-MSNs or D1-MSNs does not affect task-specific motor control. We measured nosepoke duration (time of nosepoke entry to exit) on switch responses. During interval timing there was no effect of optogenetic inhibition (red) of dorsomedial striatal D2-MSNs on A-B) nosepoke duration or C) the traversal time between the first and second nosepokes; note that traversal time is distinct from the switch response, which is the moment animals depart the first nosepoke prior to arriving at the second nosepoke. There was also no effect of optogenetic inhibition (blue) of dorsomedial striatal D1-MSNs on nosepoke duration (D-E) or F) switch traversal time. Data from the same 10 D2-Cre mice and 6 D1-Cre mice, as in Fig 5. Horizontal black lines in B, C, E, and F represent group medians.

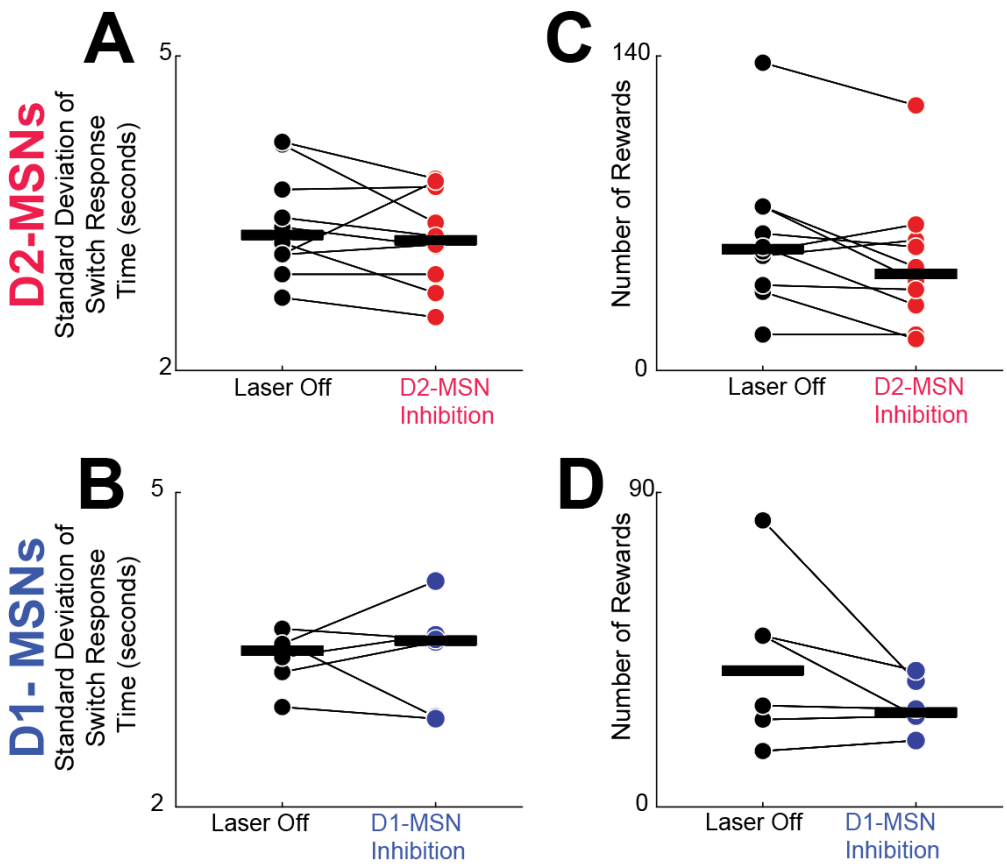

Figure S9: A) Standard deviation of switch response times for D2-MSN inhibition sessions (signed rank test, $p = 0.19$) and B) D1-MSN inhibition sessions ($p = 0.84$), and the number of total rewards for C) D2-MSN inhibition sessions ($p = 0.07$) and d) D1-MSN inhibition sessions ($p = 0.25$). Data from 10 D2-Cre mice and 6 D1-Cre mice as in Fig 5.

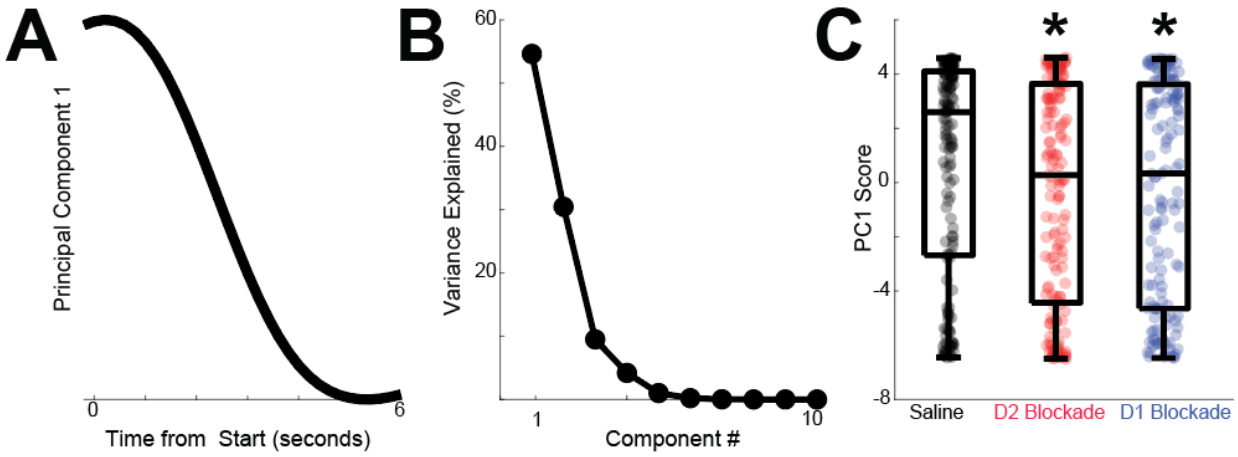

Figure S10: We analyzed MSN ensembles in sessions with saline (158 neurons), D2 blockade (167 neurons), or D1 blockade (144 neurons) – unlike Figure 6; all sessions were sorted independently and assumed to be fully statistically independent. A) Principal component analysis (PCA) identified MSN ensemble patterns of activity. The first principal component (PC1) exhibited time-dependent ramping. B) PC1 explained 55% of population variance among MSN ensembles. C) PC1 scores were shifted and significantly different with D2 or D1 blockade as when all sessions were sorted together in Fig 6. * = $p < 0.05$ via linear mixed effects models accounting for variance between mice; all analyses assumed statistical independence.

REFERENCES

Albin RL, Young AB, Penney JB. 1989. The functional anatomy of basal ganglia disorders. *Trends Neurosci* **12**:366–375. doi:10.1016/0166-2236(89)90074-X

Alexander GE, Crutcher MD. 1990. Functional architecture of basal ganglia circuits: neural substrates of parallel processing. *Trends Neurosci* **13**:266–271. doi:10.1016/0166-2236(90)90107-L

Andreasen NC. 1999. Understanding the causes of schizophrenia. *N Engl J Med* **340**:645–647. doi:10.1056/NEJM199902253400811

Averbeck BB, Lehman J, Jacobson M, Haber SN. 2014. Estimates of projection overlap and zones of convergence within frontal-striatal circuits. *J Neurosci* **34**:9497–9505.

Balci F, Gallistel CR. 2006. Cross-domain transfer of quantitative discriminations: Is it all a matter of proportion? *Psychon Bull Rev* **13**:636–642. doi:10.3758/BF03193974

Balci F, Papachristos EB, Gallistel CR, Brunner D, Gibson J, Shumyatsky GP. 2008. Interval timing in genetically modified mice: a simple paradigm. *Genes Brain Behav* **7**:373–384. doi:10.1111/j.1601-183X.2007.00348.x

Berke JD. 2011. Functional properties of striatal fast-spiking interneurons. *Front Syst Neurosci* **5**:45.

Bruce RA, Weber MA, Volkman RA, Oya M, Emmons EB, Kim Y, Narayanan NS. 2021. Experience-related enhancements in striatal temporal encoding. *Eur J Neurosci* **54**:5063–5074. doi:10.1111/ejn.15344

Buhusi CV, Meck WH. 2005. What makes us tick? Functional and neural mechanisms of interval timing. *Nat Rev Neurosci* **6**:755–765. doi:10.1038/nrn1764

Cruz BF, Guiomar G, Soares S, Motiwala A, Machens CK, Paton JJ. 2022. Action suppression reveals opponent parallel control via striatal circuits. *Nature* **607**:521–526. doi:10.1038/s41586-022-04894-9

Cui G, Jun SB, Jin X, Pham MD, Vogel SS, Lovinger DM, Costa RM. 2013. Concurrent activation of striatal direct and indirect pathways during action initiation. *Nature* **494**:238–242. doi:10.1038/nature11846

De Corte BJ, Wagner LM, Matell MS, Narayanan NS. 2019a. Striatal dopamine and the temporal control of behavior. *Behav Brain Res* **356**:375–379. doi:10.1016/j.bbr.2018.08.030

De Corte BJ, Wagner LM, Matell MS, Narayanan NS. 2019b. Striatal dopamine and the temporal control of behavior. *Behav Brain Res* **356**:375–379. doi:10.1016/j.bbr.2018.08.030

Drew MR, Fairhurst S, Malapani C, Horvitz JC, Balsam PD. 2003. Effects of dopamine antagonists on the timing of two intervals. *Pharmacol Biochem Behav* **75**:9–15.

Drew MR, Simpson EH, Kellendonk C, Herzberg WG, Lipatova O, Fairhurst S, Kandel ER, Malapani C, Balsam PD. 2007. Transient Overexpression of Striatal D2 Receptors Impairs Operant Motivation and Interval Timing. *J Neurosci* **27**:7731–7739. doi:10.1523/JNEUROSCI.1736-07.2007

Emmons EB, De Corte BJ, Kim Y, Parker KL, Matell MS, Narayanan NS. 2017. Rodent medial frontal control of temporal processing in the dorsomedial striatum. *J Neurosci* **37**:8718–8733.

Emmons EB, Kennedy M, Kim Y, Narayanan NS. 2019. Corticostriatal stimulation compensates for medial frontal inactivation during interval timing. *Sci Rep* **9**:1–9. doi:10.1038/s41598-019-50975-7

Emmons EB, Tunes-Chiuffa G, Choi J, Bruce RA, Weber MA, Kim Y, Narayanan NS. 2020. Temporal Learning Among Prefrontal and Striatal Ensembles. *Cereb Cortex Commun* **1**. doi:10.1093/texcom/tgaa058

Gouvea TS, Monteiro T, Motiwala A, Soares S, Machens C, Paton JJ. 2015. Striatal dynamics explain duration judgments. *eLife* **4**. doi:10.7554/eLife.11386

Graybiel AM. 1997. The Basal Ganglia and Cognitive Pattern Generators. *Schizophr Bull* **23**:459–469. doi:10.1093/schbul/23.3.459

Gür E, Duyan YA, Arkan S, Karson A, Balcı F. 2020. Interval timing deficits and their neurobiological correlates in aging mice. *Neurobiol Aging* **90**:33–42. doi:10.1016/j.neurobiolaging.2020.02.021

Hinton SC, Paulsen JS, Hoffmann RG, Reynolds NC, Zimbelman JL, Rao SM. 2007. Motor timing variability increases in preclinical Huntington's disease patients as estimated onset of motor symptoms approaches. *J Int Neuropsychol Soc* **13**:539–543. doi:10.1017/S1355617707070671

Kim Y-C, Han S-W, Alberico SL, Ruggiero RN, De Corte B, Chen K-H, Narayanan NS. 2017a. Optogenetic Stimulation of Frontal D1 Neurons Compensates for Impaired Temporal Control of Action in Dopamine-Depleted Mice. *Curr Biol CB* **27**:39–47. doi:10.1016/j.cub.2016.11.029

Kim Y-C, Han S-W, Alberico SL, Ruggiero RN, De Corte B, Chen K-H, Narayanan NS. 2017b. Optogenetic stimulation of frontal D1 neurons compensates for impaired temporal control of action in dopamine-depleted mice. *Curr Biol* **27**:39–47.

Kravitz AV, Freeze BS, Parker PR, Kay K, Thwin MT, Deisseroth K, Kreitzer AC. 2010. Regulation of parkinsonian motor behaviours by optogenetic control of basal ganglia circuitry. *Nature* **466**:622–626.

Larson T, Khandelwal V, Weber MA, Leidinger MR, Meyerholz DK, Narayanan NS, Zhang Q. 2022. Mice expressing P301S mutant human tau have deficits in interval timing. *Behav Brain Res* **432**:113967. doi:10.1016/j.bbr.2022.113967

Latimer KW, Yates JL, Meister ML, Huk AC, Pillow JW. 2015. Single-trial spike trains in parietal cortex reveal discrete steps during decision-making. *Science* **349**:184–187.

Matell MS, Meck WH. 2004. Cortico-striatal circuits and interval timing: coincidence detection of oscillatory processes. *Cogn Brain Res*, Neuroimaging of Interval Timing **21**:139–170. doi:10.1016/j.cogbrainres.2004.06.012

Matell MS, Meck WH, Nicolelis MAL. 2003. Interval timing and the encoding of signal duration by ensembles of cortical and striatal neurons. *Behav Neurosci* **117**:760–773. doi:10.1037/0735-7044.117.4.760

Meck WH. 2006. Neuroanatomical localization of an internal clock: A functional link between mesolimbic, nigrostriatal, and mesocortical dopaminergic systems. *Brain Res* **1109**:93–107. doi:10.1016/j.brainres.2006.06.031

Mello GBM, Soares S, Paton JJ. 2015. A Scalable Population Code for Time in the Striatum. *Curr Biol* **25**:1113–1122. doi:10.1016/j.cub.2015.02.036

Merchant H, de Lafuente V. 2014. Introduction to the neurobiology of interval timing. *Adv Exp Med Biol* **829**:1–13. doi:10.1007/978-1-4939-1782-2_1

Middleton FA, Strick PL. 2000. Basal ganglia and cerebellar loops: motor and cognitive circuits. *Brain Res Rev* **31**:236–250. doi:10.1016/S0165-0173(99)00040-5

Monteiro T, Rodrigues FS, Pexirra M, Cruz BF, Gonçalves AI, Rueda-Orozco PE, Paton JJ. 2023. Using temperature to analyze the neural basis of a time-based decision. *Nat Neurosci*. doi:10.1038/s41593-023-01378-5

Narayanan NS. 2016. Ramping activity is a cortical mechanism of temporal control of action. *Curr Opin Behav Sci* **8**:226–230. doi:10.1016/j.cobeha.2016.02.017

Narayanan NS, Albin RL. 2022. Cognition in Parkinson's Disease, Progress in Brain Research. Elsevier, Acad. Press.

Narayanan NS, Cavanagh JF, Frank MJ, Laubach M. 2013. Common medial frontal mechanisms of adaptive control in humans and rodents. *Nat Neurosci* **16**:1888–1897. doi:10.1038/nn.3549

Narayanan NS, Laubach M. 2009. Delay activity in rodent frontal cortex during a simple reaction time task. *J Neurophysiol* **101**:2859–2871. doi:10.1152/jn.90615.2008

Nguyen Q-A, Rinzel J, Curtu R. 2020. Buildup and bistability in auditory streaming as an evidence accumulation process with saturation. *PLOS Comput Biol* **16**:e1008152. doi:10.1371/journal.pcbi.1008152

Parker KL, Chen K-H, Kingyon JR, Cavanagh JF, Narayanan NS. 2015. Medial frontal ∼4-Hz activity in humans and rodents is attenuated in PD patients and in rodents with cortical dopamine depletion. *J Neurophysiol* **114**:1310–1320. doi:10.1152/jn.00412.2015

Parker KL, Chen K-H, Kingyon JR, Cavanagh JF, Narayanan NS. 2014. D1-Dependent 4 Hz Oscillations and Ramping Activity in Rodent Medial Frontal Cortex during Interval Timing. *J Neurosci* **34**:16774–16783. doi:10.1523/JNEUROSCI.2772-14.2014

Parker KL, Kim YC, Kelley RM, Nessler AJ, Chen K-H, Muller-Ewald VA, Andreasen NC, Narayanan NS. 2017. Delta-frequency stimulation of cerebellar projections can compensate for schizophrenia-related medial frontal dysfunction. *Mol Psychiatry* **22**:647–655. doi:10.1038/mp.2017.50

Parker KL, Lamichhane D, Caetano MS, Narayanan NS. 2013. Executive dysfunction in Parkinson's disease and timing deficits. *Front Integr Neurosci* **7**:75. doi:10.3389/fnint.2013.00075

Paton JJ, Buonomano DV. 2018. The Neural Basis of Timing: Distributed Mechanisms for Diverse Functions. *Neuron* **98**:687–705. doi:10.1016/j.neuron.2018.03.045

Robbe D. 2023. Lost in time: Relocating the perception of duration outside the brain. *Neurosci Biobehav Rev* **153**:105312. doi:10.1016/j.neubiorev.2023.105312

Ryan MB, Bair-Marshall C, Nelson AB. 2018. Aberrant striatal activity in parkinsonism and levodopa-induced dyskinesia. *Cell Rep* **23**:3438–3446.

Shepherd GMG. 2013. Corticostriatal connectivity and its role in disease. *Nat Rev Neurosci* **14**:278–291. doi:10.1038/nrn3469

Shimazaki H, Shinomoto S. 2007. A Method for Selecting the Bin Size of a Time Histogram. *Neural Comput* **19**:1503–1527. doi:10.1162/neco.2007.19.6.1503

Shin JH, Kim D, Jung MW. 2018. Differential coding of reward and movement information in the dorsomedial striatal direct and indirect pathways. *Nat Commun* **9**:1–14.

Simen P, Balci F, de Souza L, Cohen JD, Holmes P. 2011. A model of interval timing by neural integration. *J Neurosci Off J Soc Neurosci* **31**:9238–9253. doi:10.1523/JNEUROSCI.3121-10.2011

Singh A, Cole RC, Espinoza AI, Evans A, Cao S, Cavanagh JF, Narayanan NS. 2021. Timing variability and midfrontal ~4 Hz rhythms correlate with cognition in Parkinson's disease. *NPJ Park Dis* **7**:14. doi:10.1038/s41531-021-00158-x

Soares S, Atallah BV, Paton JJ. 2016. Midbrain dopamine neurons control judgment of time. *Science* **354**:1273–1277. doi:10.1126/science.aah5234

Stutt HR, Weber MA, Cole RC, Bova AS, Ding X, McMurrin MS, Narayanan NS. 2024. Sex similarities and dopaminergic differences in interval timing. *Behav Neurosci* **138**:85–93. doi:10.1037/bne0000577

Tecuapetla F, Jin X, Lima SQ, Costa RM. 2016. Complementary Contributions of Striatal Projection Pathways to Action Initiation and Execution. *Cell* **166**:703–715. doi:10.1016/j.cell.2016.06.032

Toda K, Lusk NA, Watson GDR, Kim N, Lu D, Li HE, Meck WH, Yin HH. 2017. Nigrotectal Stimulation Stops Interval Timing in Mice. *Curr Biol* **27**:3763-3770.e3. doi:10.1016/j.cub.2017.11.003

Tosun T, Gur E, Balci F. 2016. Mice plan decision strategies based on previously learned time intervals, locations, and probabilities. *Proc Natl Acad Sci U S A* **113**:787–792. doi:10.1073/pnas.1518316113

Wang J, Narain D, Hosseini EA, Jazayeri M. 2018. Flexible timing by temporal scaling of cortical responses. *Nat Neurosci* **21**:102. doi:10.1038/s41593-017-0028-6

Ward RD, Kellendonk C, Kandel ER, Balsam PD. 2011. Timing as a window on cognition in schizophrenia. *Neuropharmacology*. doi:10.1016/j.neuropharm.2011.04.014

Weber MA, Kerr G, Thangavel R, Conlon MM, Gumusoglu SB, Gupta K, Abdelmotilib HA, Halhouli O, Zhang Q, Geerling JC, Narayanan NS, Aldridge GM. 2024. Alpha-Synuclein Pre-Formed Fibrils Injected into Prefrontal Cortex Primarily Spread to Cortical and Subcortical Structures. *J Park Dis* **14**:81–94. doi:10.3233/JPD-230129

Weber MA, Sivakumar K, Tabakovic EE, Oya M, Aldridge GM, Zhang Q, Simmering JE, Narayanan NS. 2023. Glycolysis-enhancing α1-adrenergic antagonists modify cognitive symptoms related to Parkinson's disease. *Npj Park Dis* **9**:1–7. doi:10.1038/s41531-023-00477-1

Yun S, Yang B, Anair JD, Martin MM, Fleps SW, Pamukcu A, Yeh N-H, Contractor A, Kennedy A, Parker JG. 2023. Antipsychotic drug efficacy correlates with the modulation of D1 rather than D2 receptor-expressing striatal projection neurons. *Nat Neurosci* 1–12. doi:10.1038/s41593-023-01390-9

Zhang Q, Abdelmotilib H, Larson T, Keomanivong C, Conlon M, Aldridge GM, Narayanan NS. 2021. Cortical alpha-synuclein preformed fibrils do not affect interval timing in mice. *Neurosci Lett* **765**:136273. doi:10.1016/j.neulet.2021.136273